Hindawi Publishing Corporation
Advances in Condensed Matter Physics
Volume 2013, Article ID 104379, 25 pages
http://dx.doi.org/10.1155/2013/104379

Review Article

Electrodynamics of Metallic Superconductors

M. Dressel

1. Physikalisches Institut, Universität Stuttgart, Pfaffenwaldring 57, 70550 Stuttgart, Germany

Correspondence should be addressed to M. Dressel; dressel@pi1.physik.uni-stuttgart.de

Received 11 April 2013; Revised 23 May 2013; Accepted 9 June 2013

Academic Editor: Victor V. Moshchalkov

The theoretical and experimental aspects of the microwave, terahertz, and infrared properties of superconductors are discussed. Electrodynamics can provide information about the superconducting condensate as well as about the quasiparticles. The aim is to understand the frequency dependence of the complex conductivity, the change with temperature and time, and its dependence on material parameters. We confine ourselves to conventional metallic superconductors, in particular, Nb and related nitrides and review the seminal papers but also highlight latest developments and recent experimental achievements. The possibility to produce well-defined thin films of metallic superconductors that can be tuned in their properties allows the exploration of fundamental issues, such as the superconductor-insulator transition; furthermore it provides the basis for the development of novel and advanced applications, for instance, superconducting single-photon detectors.

1. Introduction

1.1. Historical Developments. The history of superconductivity in the 1950s is one of the best examples of how the interplay of experiment and theory advances science towards a profound understanding. After having moved to Urbana in 1951 and even more intense after having received the Nobel Prize for the development of the transistor in 1956, John Bardeen was pressing to solve the longstanding problem of superconductivity. During these years he was very well aware of the experimental facts and recent developments but also triggered experimental investigations and pushed certain measurements.

The presence of an energy gap in the density of states of a superconductor (and thus in the excitation spectrum) can be inferred from the temperature dependence of the specific heat that had been measured already in Heike Kamerlingh Onnes' laboratory in Leiden [1]; however, it was Bardeen who seriously discussed this idea in more detail in 1955 [2, 3] based on considerations proposed by Welker [4] years earlier. He assumed "that in the superconducting state a finite energy gap $\Delta \approx k_B T_c$ is required to excite electrons from the surface of the Fermi sea." Cooper developed this concept further when he introduced the electron pairs in the following year [5]. In the seminal BCS paper of 1957 [6], Bardeen, Cooper and Schrieffer finally derived the fundamental ratio $2\Delta/k_B T_c = 3.5$ and the temperature dependence of the energy gap. In their calculation of the matrix elements, they explicitly refer to the ongoing NMR relaxation-rate experiments by Hebel and Slichter [7, 8], ultrasound-attenuation measurements by Morse and Bohm [9], and microwave-absorption experiments by the Tinkham group [10–12].

Concerning the high-frequency absorption, in an article submitted 1955 [13] Buckingham suggested that (for consistency reasons the notation is transformed):

> *"a gap of width* $2\Delta(0)$ *in the electron energy spectrum in the ground state, its width,* 2Δ*, at finite temperatures will decrease, eventually vanishing at the transition temperature,* T_c*. The normal state is regarded as one in which the energy spectrum is without a gap and is independent of temperature, the system representing the superconducting state becoming identical with the normal one for* $T > T_c$*. The electromagnetic properties of such a system will depend strongly on the size of the gap, but at high frequencies and near the transition*

temperature, when $\hbar\omega/2\Delta$ is large, will approach those of the normal state (without gap)."

Looking at the experimental results of Blevins et al. who measured the surface resistance of tin in the millimeter-wave range [14], he suggested some scaling of frequency and transition temperature close to T_c. This was further developed by Tinkham [11], based on his far-infrared transmission measurements on thin lead films [10] where an anomalously high transmission was observed (cf. Figure 1(b)). He suggested two contributions (superconducting and normal electrons) becoming relevant in the limiting cases of low and high frequencies:

"*We consider a model of a superconductor at absolute zero in which a gap of width $\hbar\omega_g \approx 3k_BT_c$ appears in the spectrum of one-electron energy states. [$\cdots$] The lossy conductivity σ_1 will be zero for photon energies $\hbar\omega < \hbar\omega_g$. For $\omega > \omega_g$, σ_1 will rise gradually with ω as an increasing fraction of the states originally within $\hbar\omega$ of the occupied states below the Fermi level are still available for excitation. If the gap merely excluded the states within $\hbar\omega_g$ leaving all else unchanged, this simple picture would suggest a rise as $\sigma_1 = \sigma_n(1-\omega_g/\omega)$. The experimental rise seems to be faster, cutting off at least as fast as $(1-\omega_g^2/\omega^2)$. This might correspond to the states displaced from the gap just "piling up" on either side, so that the change averages to zero more rapidly for $\omega \gg \omega_g$.*"

These ideas are further developed and extended in later papers [12, 15], where the size of the superconducting energy gap and the shape $\sigma_1(\omega)$ at ω_g were analyzed using data of different materials [16].

The situation was more or less settled in 1958, when the Westinghouse group of Biondi et al. summarized the situation on the superconducting energy gap in a review [17]. Previously they had published several thorough microwave and millimeter-wave results on superconducting aluminum and tin [18–20], and several nice papers followed [21–23]. At the same time Tinkham gave an overview on the work of his group [24]. While Biondi and Garfunkel always measured the temperature dependence for certain frequencies, Tinkham and his collaborators focussed at the spectral properties at fixed temperatures. This allowed him to make the sum-rule argument introduced in the previous quote [11], which was finalized by Ferrell et al. in 1959 [25, 26]. In Figure 1 the frequency dependence of the electrodynamical properties of a superconductor at $T = 0$ is sketched. Upon decreasing the frequency the real part of the conductivity $\sigma_1(\omega)/\sigma_n$ gradually vanishes at the gap frequency $\omega_g = 2\Delta/\hbar$, while the imaginary part $\sigma_2(\omega)/\sigma_n$ diverges as $\omega \to 0$. The maximum in the relative transmission $\mathrm{Tr}_s/\mathrm{Tr}_n$ is observed right at the gap (with values well above the unity) before it goes to zero for $\omega = 0$. There is also a maximum of the absorption above the superconducting gap, but no absorption takes place below the gap 2Δ. It poses a real challenge to measure the reflectivity of a metallic superconductor since it approaches unity at ω_g, but in general it is well above 99% already in the normal state (Figure 1(c)).

The problem remaining was the determination of the superconducting conductivity, that is, the actual frequency and temperature dependence of $\sigma_1(\omega)$ and $\sigma_2(\omega)$ individually without the assumption of any model or Kramers-Kronig relation. Figure 2 displays temperature and frequency-dependent conductivity σ_1/σ_n as it is calculated from Mattis-Bardeen theory. σ_1/σ_n features a minimum at $\hbar\omega/2\Delta(T) = 1$ which shifts to lower frequencies and is smeared out as T approaches T_c from below. Also seen is the enormous enhancement of the conductivity $\sigma_1(\omega)/\sigma_n$ for low frequencies observed right below the superconducting gap: it became known as the coherence peak. Despite continuous efforts over the years [30–32], only in 1968 Palmer and Tinkham reached this goal of measuring the real and imaginary parts of the electrodynamic response independently [33]; simultaneous measurements of the far-infrared transmission through and reflection off thin films of lead made it possible to calculate the conductivity unambiguously. The status is summarized in several reviews [34, 35]. The precise measurement of the temperature-dependent conductivity right below the superconducting transition, however, was achieved only a quarter of a century later in the group of Grüner [36, 37]. Previous efforts by the Cambridge group of Pippard and others were less convincing [38–40]. The so-called coherence peak known from the NMR experiments of Hebel and Slichter [7, 8] is also seen in the microwave conductivity of lead, niobium, and eventually even in alumimum [29] where for the first time the complete frequency evolution of the coherence peak was measured; exactly fifty years after it was calculated. Still ultrasound absorption remains a desideratum in the exploration of the coherence effects: a peak is predicted above 2Δ, but no frequency-dependent ultrasound absorption measurements on superconductors have been carried out in the vicinity of the energy gap.

Even today, Tinkham's book [41–43] gives the best introduction to the electrodymical properties of conventional superconductors. More detailed descriptions can be found by Rickayzen [44] and Parks [45] or more recent textbooks [46].

1.2. Recent Developments. Having understood the bulk properties of metallic superconductors fairly well, there are still many open questions when going to the vortex lattice, very thin films, nanostructures, inhomogeneous materials, granular superconductors, highly disordered films and so forth, which are subject of today's research efforts. Thin films of metallic superconductors are of both technological and academic interests.

As we will see, the properties of interacting electron systems are governed by the electronic density of states [47], which changes upon reducing spatial dimensions. Thus, dimensional reduction from three dimensions to two dimensions (3D $\to$ 2D) may affect optical, electronic, and thermodynamic properties of the system. In superconductivity, studying quasi-two-dimensional thin-film systems turns out to be a particularly fruitful field and leads to remarkable findings such as insulators featuring a superconducting gap [48],

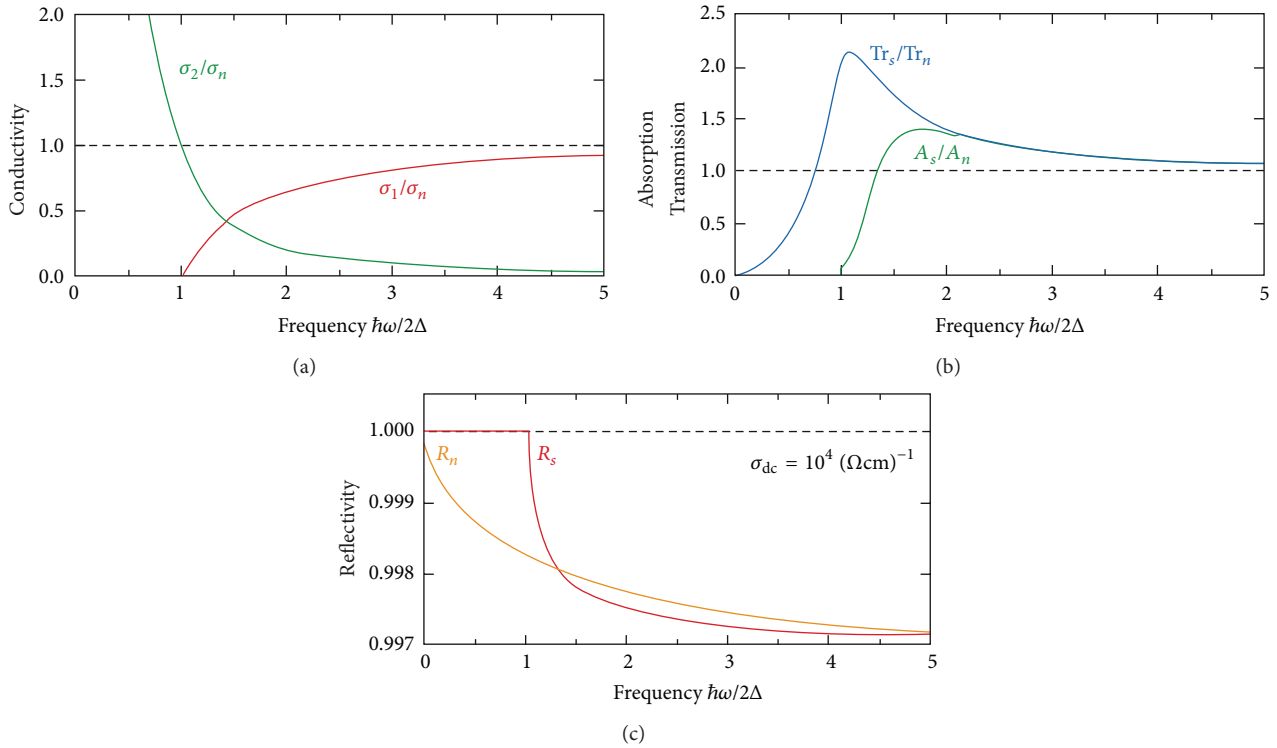

FIGURE 1: Sketch of the electrodynamic properties of a superconductor at $T = 0$: (a) in the upper panel the frequency dependence of the real and imaginary parts of the conductivity σ_1 and σ_2 is plotted, normalized to the normal state behavior σ_n, which basically can be assumed to be constant in the spectral range of interest, where $\omega \ll \Gamma$ with Γ the quasiparticle scattering rate. (b) The second panel exhibits the frequency dependence of the relative transmission $\mathrm{Tr}_s/\mathrm{Tr}_n$ and absorption A_s/A_n. (c) The optical reflectivity of a superconductor R_s is compared to the reflectivity of a normal metal R_n, assuming a dc conductivity of $10^4\ (\Omega\mathrm{cm})^{-1}$.

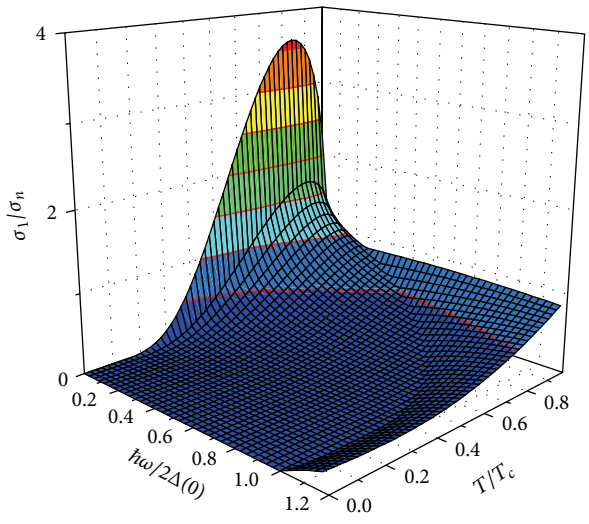

FIGURE 2: Frequency and temperature dependence of the real part of the conductivity σ_1/σ_n calculated according the BCS theory [27, 28] with the ratio of the coherence length to the mean free path $\pi\xi(0)/2\ell = 10$. The pronounced maximum for low frequencies at a temperature slightly below T_c is the coherence peak. The kink at $\hbar\omega = 2\Delta(0)$ corresponds to the superconducting gap that decreases with temperature and vanishes for $T \to T_c$ (after [29]).

pseudogap in conventional s-wave superconductors [49], or extremely strong-coupling superconductivity in Kondo lattices [50]. NbN has recently gained attention as a model system for the superconductor-insulator transition; a topic intensively investigated in thin films of Bi, InO, or TiN: tunneling studies [51] reveal a gapped density of states slightly above T_c in highly disordered films as it has been found for TiN films [49]. This peculiar state resembles the well-established pseudogap in high-T_c cuprate superconductors [52, 53]. In case of NbN, however, T_c is about one order of magnitude higher compared to TiN. Thus, measurements on NbN in the vicinity of the superconductor-insulator transition (SIT) are much less demanding [54, 55]. Consequently, results obtained for NbN might serve as a key to understand the still puzzling pseudogap state in high-T_c cuprates.

Besides pure academic interest, thin-film superconductors play a key role in many state-of-the-art applications such as superconducting quantum interference devices (SQUID), thermal and electrical switches using Josephson junctions, or microwave resonators [56]. Contrary to nonmetallic systems such as MgB_2 or cuprates, thin and ultrathin films of NbN and TaN can be produced of very high quality, for example, by reactive dc-magneton sputtering [57, 58]. They are of particular interest due to their high critical temperature that

makes them suited for novel approaches to build single-photon detectors, for example [57, 59–63].

2. Theory

2.1. Mattis-Bardeen Theory. Based on the BCS theory [6], the description of the electrodynamic properties of a superconductor was given by Mattis and Bardeen in their seminal paper [27]. Miller applied these considerations on the surface impedance [64]. In parallel Abrikosov and coworkers [65, 66] also described the electromagnetic absorption of a superconductor, including the coherence factors and the nonlocal relationship between vector potential and induced currents.

The celebrated Mattis-Bardeen equations read

$$\frac{\sigma_1(\omega,T)}{\sigma_n} = \frac{2}{\hbar\omega}\int_{\Delta}^{\infty}\frac{\left[f(\mathscr{E})-f(\mathscr{E}+\hbar\omega)\right]\left(\mathscr{E}^2+\Delta^2+\hbar\omega\mathscr{E}\right)}{\left(\mathscr{E}^2-\Delta^2\right)^{1/2}\left[(\mathscr{E}+\hbar\omega)^2-\Delta^2\right]^{1/2}}d\mathscr{E} + \frac{1}{\hbar\omega}\int_{\Delta-\hbar\omega}^{-\Delta}\frac{\left[1-2f(\mathscr{E}+\hbar\omega)\right]\left(\mathscr{E}^2+\Delta^2+\hbar\omega\mathscr{E}\right)}{\left(\mathscr{E}^2-\Delta^2\right)^{1/2}\left[(\mathscr{E}+\hbar\omega)^2-\Delta^2\right]^{1/2}}d\mathscr{E} \tag{1}$$

$$\frac{\sigma_2(\omega,T)}{\sigma_n} = \frac{1}{\hbar\omega}\int_{\Delta-\hbar\omega,-\Delta}^{\Delta}\frac{\left[1-2f(\mathscr{E}+\hbar\omega)\right]\left(\mathscr{E}^2+\Delta^2+\hbar\omega\mathscr{E}\right)}{\left(\Delta^2-\mathscr{E}^2\right)^{1/2}\left[(\mathscr{E}+\hbar\omega)^2-\Delta^2\right]^{1/2}}d\mathscr{E}, \tag{2}$$

where for $\hbar\omega > 2\Delta$ the lower limit of the integral in (2) becomes $-\Delta$. Here $f(\mathscr{E},T) = (\exp\{\mathscr{E}/k_BT\}-1)^{-1}$ is the usual Fermi-Dirac distribution function. The expression of σ_1/σ_n describes the response of the normal carriers, that is, the dissipative part. The first term of (1) represents the effects of thermally excited quasiparticles, which vanishes for $T = 0$. The second term mainly accounts for the contribution of photon-excited quasiparticles; since it requires the breaking of a Cooper pair, it is basically zero for $\hbar\omega < 2\Delta(T)$. However, there is a small contribution possible of quasiparticles thermally excited across the gap for $T \lesssim T_c$.

The sketch in Figure 3 illustrates the electronic density of states for a normal metal (panel a), a superconductor at finite temperatures (panel b) and the superconductor at $T = 0$ (panel c). Single-particle excitations only take place from occupied states (dark colors) to empty states (light colors). In the case of a metal ($T > T_c$) this is possible for any finite photon energy $\hbar\omega$ leading to a Drude response limited only by the scattering rate $1/\tau$. When the superconducting gap opens in the density of states for $T < T_c$, the states from the gap region pile up above and below $\pm\Delta(T)$ making a large number of excitations possible. We have to distinguish excitations across the gap (solid arrows) for $\hbar\omega > 2\Delta(T)$ from those above (and correspondingly below) the gap between occupied and unoccupied states due to the finite-temperature Fermi distribution $f(\mathscr{E},T)$. The latter ones have no lower-energy limit and dominate the low-frequency response since the joint density of states is largest for $\hbar\omega \to 0$. These thermally activated contributions to the optical conductivity [first term in (1)] are shown by red dashed lines in Figure 4. They are actually observed as the coherence peak in the temperature dependent conductivity right below T_c (see Section 3.1 below). These quasiparticle excitations are limited by the occupation given by the Fermi distribution. The across-gap excitations, on the other hand, always have a clear-cut lower-frequency limit ω_g determined by the gap $2\Delta/\hbar$; this is the energy required to break a Cooper pair. In Figure 4 these excitations (second term in (1)) are plotted as blue dashed lines. Due to the case-2 coherence factor describing the quasiparticle excitations in a superconductor, the conductivity only smoothly increases for $\omega > 2\Delta/\hbar$, despite the divergency in the density of states right above and below the gap [46]. For $T = 0$ these are the only quasiparticle contributions to $\sigma_1(\omega)$. The superconducting condensate is observed as a δ-peak at $\omega = 0$ and dominates the imaginary part $\sigma_2(\omega)$. A generalized Mattis-Bardeen theory which accounts for quasiparticle scattering is derived by Zimmermann et al. [28]. The inset of Figure 4 displays how a finite scattering rate modifies $\sigma_1(\omega)$ and $\sigma_2(\omega)$.

An interesting aspect was elucidated by Chang and Scalapino [67–69], who found an enhancement of the superconducting energy gap and a change in the quasiparticle density of states upon microwave irradiation, in addition to a redistribution of quasiparticles by the microwaves. Eventually it extends to the field of nonequilibrium superconductivity that has been a widely studied field for half a century [70, 71].

Already from the London equations, a relation between the imaginary part of the conductivity and the London penetration depth is obtained [46]:

$$\sigma_2(\omega) = \frac{Ne^2}{m\omega} = \frac{c^2}{4\pi\lambda_L^2\omega}, \tag{3}$$

where the London penetration $\lambda_L = (mc^2/4\pi N_s e^2)^{1/2}$ is determined by the superconducting charge carrier mass and density, m and N_s. Through the Kramers-Kronig relation the real part of the conductivity is then given by

$$\sigma_1(\omega) = \frac{\pi}{2}\frac{N_s e^2}{m}\delta\{\omega=0\} = \frac{c^2}{8\lambda_L^2}\delta\{\omega=0\}, \tag{4}$$

where $\delta\omega = 0$ denote a delta peak centered at $\omega = 0$.

Figures 5 and 6 summarize the frequency and temperature dependence of σ_1 and σ_2 as derived from (1) and (2) assuming the finite scattering effects $\pi\xi(0)/\ell = 10$ discussed in [28, 73–77]. Although the density of states diverges at $\pm\Delta$, the conductivity $\sigma_1(\omega)$ does not show a divergency but a smooth increase which follows approximately the dependence $\sigma_1(\omega)/\sigma_n \propto 1-(\hbar\omega/k_BT_c)^{-1.65}$. The temperature dependent conductivity $\sigma_1(T)$ shows a peak just below T_c at a low frequency; the maximum occurs around $0.8T_c$ and slightly shifts up with frequency. It is called the coherence peak because it does not just reflect the enhanced density of states but is also an expression of the quantum mechanical

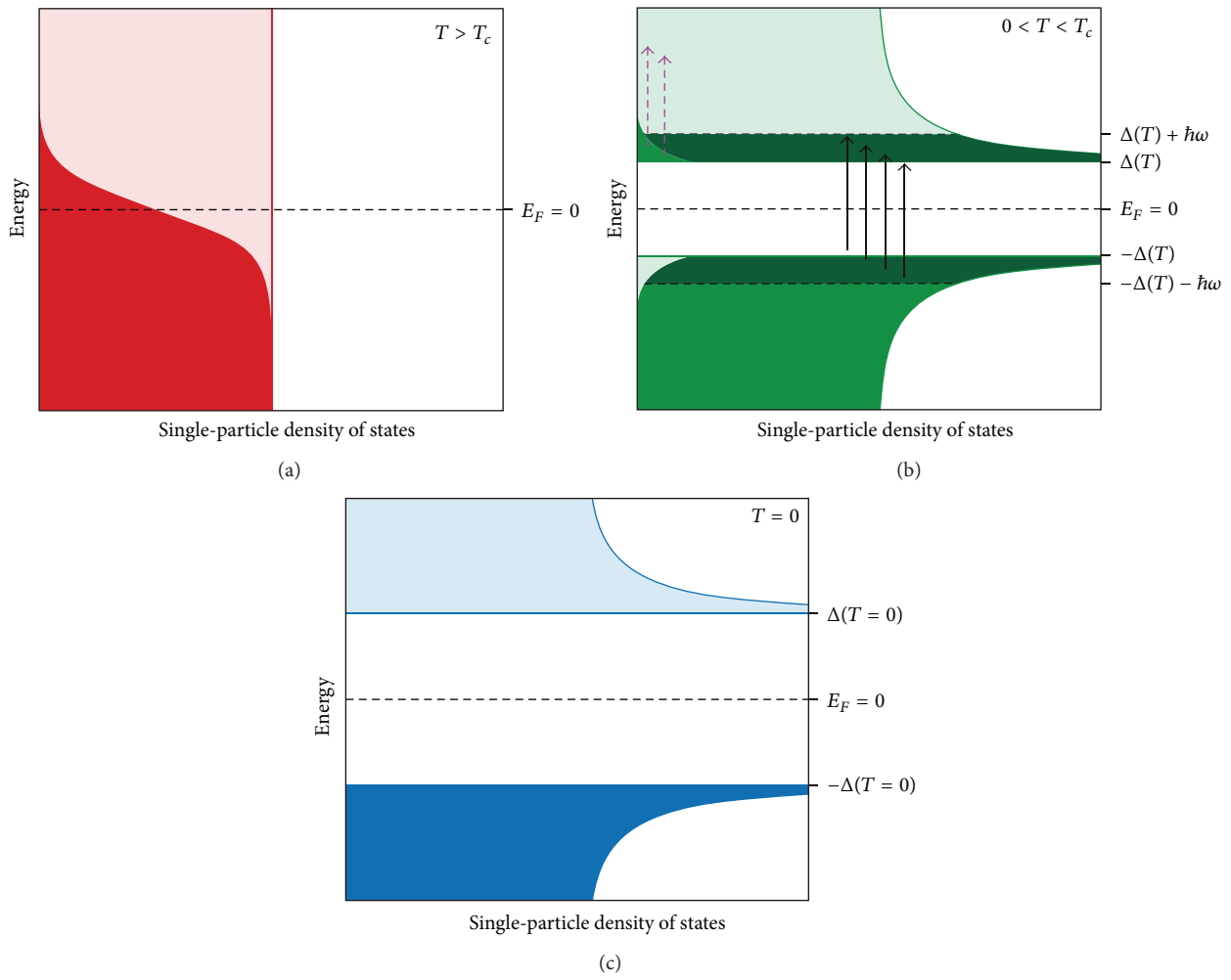

FIGURE 3: The density of electronic states in the close vicinity of the Fermi energy E_F. (a) For a normal metal, the density of states is basically constant. The dark colored area indicates the occupied states according to the Fermi-Dirac statistic at finite temperature. (b) In the case of a superconductor, an energy gap opens around E_F; it grows continuously as the temperature is reduced below T_c. The dotted arrow indicates possible excitations of the occupied states above the gap [first term in (1)], leading to a quasiparticle peak at $\omega = 0$. For the electronic excitations shown by the solid arrow, a minimum energy of 2Δ is required; their contribution is captured by the second term in (1). The dark shaded area up to $|\Delta(T) + \hbar\omega|$ indicates states that can contribute to the conductivity by absorption of photons of arbitrary energy $\hbar\omega$. (c) The full size of the superconducting energy gap is given by $2\Delta_0$ for $T = 0$. No quasiparticle peak is present, leading to absorption only above $\omega_g = 2\Delta/\hbar$. The states removed from the gap area are pilled up below and above the gap, leading to a $E/\sqrt{E^2 - \Delta_0^2}$ divergency.

factor relevant for these excitations. The so-called coherence factor $F(\mathscr{E}_{\mathbf{k}}, \mathscr{E}_{\mathbf{k}'})$ describes the scattering of a quasiparticle from a state $\mathbf{k}$ with energy $\mathscr{E}_{\mathbf{k}}$ to a state $\mathbf{k}' = \mathbf{k} + \mathbf{q}$ with energy $\mathscr{E}_{\mathbf{k}'} = \mathscr{E}_{\mathbf{k}} + \hbar\omega$ upon absorption of a photon with energy $\hbar\omega$ and momentum $\mathbf{q}$. If summed over all $\mathbf{k}$ values, it reads [41–43, 46]

$$F\left(\Delta, \mathscr{E}, \mathscr{E}'\right) = \frac{1}{2}\left(1 + \frac{\Delta^2}{\mathscr{E}\mathscr{E}'}\right). \tag{5}$$

Only for energies below the gap 2Δ, this factor is appreciable: $F \approx 1$ for $\hbar\omega \ll 2\Delta$. For $\hbar\omega \geq 2\Delta$, the coherence factors are reversed, and F vanishes in the present case. For large energies, the coherence effects become negligible since $\mathscr{E}, \mathscr{E}' \gg 2\Delta$ and $F \approx 1/2$. Hence the coherence peak is seen as a maximum in $\sigma_1(T)$ in the low-frequency limit; it becomes smaller with increasing frequency and shifts to higher temperatures. The height of the peak has the following frequency dependence:

$$\left(\frac{\sigma_1}{\sigma_n}\right)_{\max} \sim \log\left\{\frac{2\Delta(0)}{\hbar\omega}\right\}. \tag{6}$$

The peak disappears completely for $\hbar\omega \geq \Delta/2$ (well below 2Δ). At $T = 0$ and $\omega < 2\Delta/\hbar$ the complex part of the conductivity σ_2/σ_n describes the response of the Cooper pairs and is related to the gap parameter through the expression

$$\frac{\sigma_2(T)}{\sigma_n} \approx \frac{\pi\Delta(T)}{\hbar\omega}\tanh\left\{\frac{\Delta(T)}{2k_BT}\right\} \approx \lim_{T\to 0}\frac{\pi\Delta(0)}{\hbar\omega}. \tag{7}$$

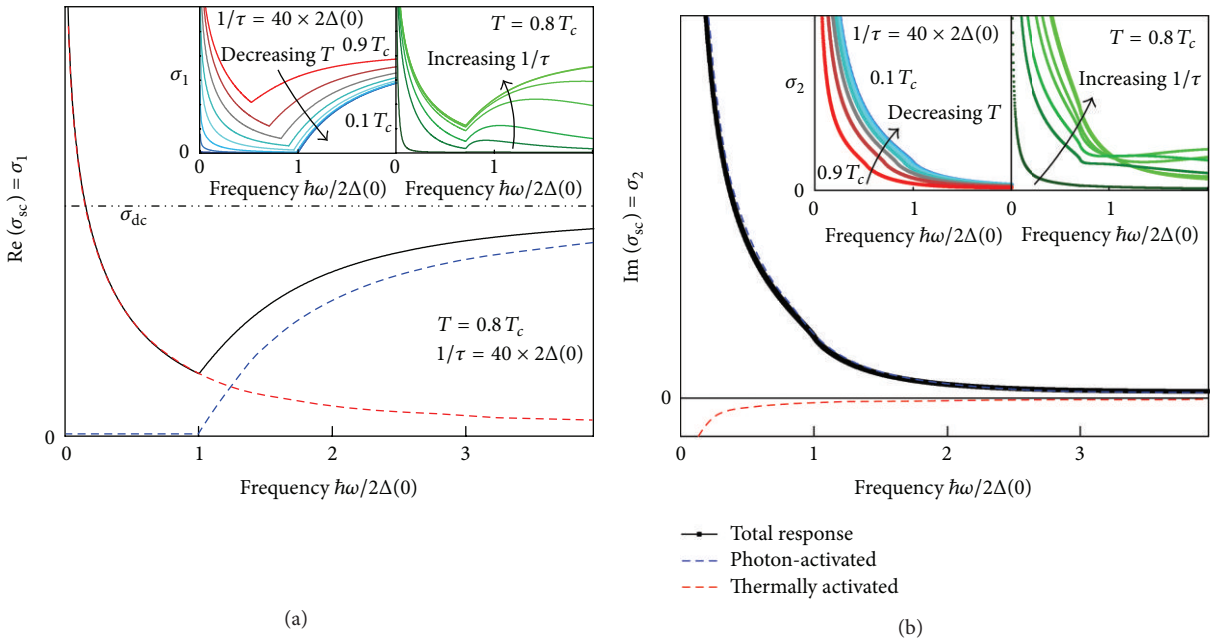

FIGURE 4: (a) Real and (b) imaginary parts of the complex optical conductivity (solid line) of a superconductor as a function of frequency based on generalized Mattis-Bardeen theory [27] for $T = 0.8T_c$ and a finite scattering rate [28]. Dashed lines disentangle the contributions of both the thermal electrons [first term in (1) and dashed arrows in Figure 3(b)] and photon-activated electrons [second term in (1) and solid arrow in Figure 3(b)] to the conductivity. Insets of (a) and (b) show σ_1 and σ_2 for different temperatures (T/T_c = 0.9, 0.8, 0.7, 0.6, 0.5, 0.4, 0.3, 0.2, and 0.1) and scattering rates ($1/\tau$ = 40, 20, 4, 2, 0.8, 0.4, and $0.04 \times 2\Delta(0)/\hbar$), respectively. (Used parameters $2\Delta(0)/hc = 25\,\text{cm}^{-1}$, $T_c = 10\,\text{K}$, and $\sigma_{dc} = 1066\,\Omega^{-1}\,\text{cm}^{-1}$) (after [72]).

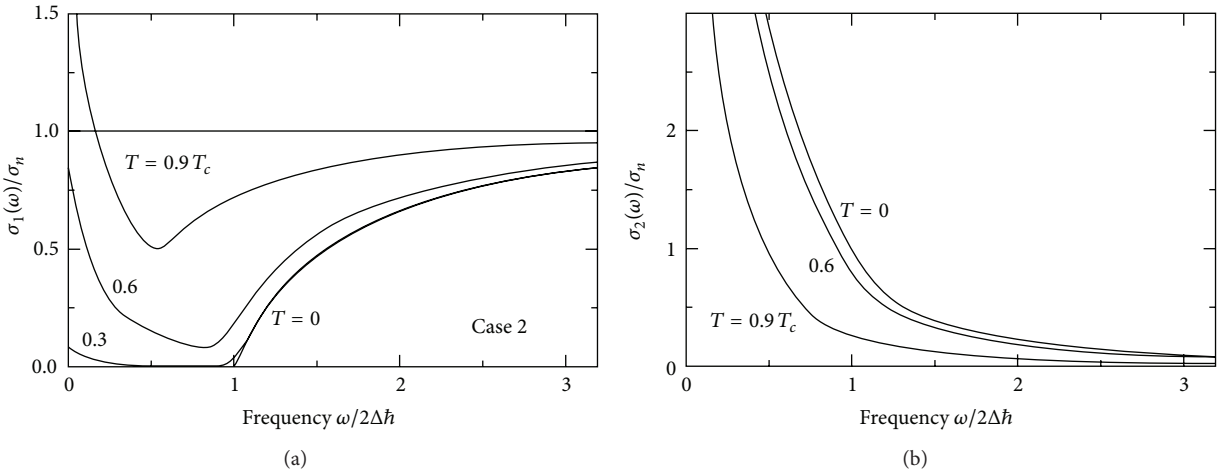

FIGURE 5: Frequency dependence of the conductivity of a superconductor at different temperatures T relative to the transition temperature T_c. (a) The real part $\sigma_1(\omega)/\sigma_n$ exhibits a sharp drop at the superconducting gap 2Δ and vanishes below for $T = 0$. For finite temperatures, the gap gradually moves to lower frequencies; in addition a finite conductivity emerges at low frequencies that increases considerably as $T \to T_c$; σ_1 even exceeds the normal state conductivity in a narrow frequency range right below T_c. (b) The imaginary part of the conductivity $\sigma_2(\omega)/\sigma_n$ diverges for low temperatures as $\sigma_2(\omega) \propto \omega^{-1}$. The kink of $\sigma_1(\omega)$ at $\omega = 2\Delta/\hbar$ also shows up in the imaginary part $\sigma_2(\omega)$ [46].

2.2. Scattering Effects, Length Scales, and Sum Rule. The Equations (1) and (2) were derived by Mattis and Bardeen [27] assuming the infinite scattering time $\tau \to \infty$. In 1967 Nam showed [76, 77], however, that these equations are more general and also valid for $\tau \to 0$. He also extended the application towards the strong coupling regime: $2\Delta/k_BT_c > 3.53$. Nevertheless, in order to describe the electrodynamics of superconductors, different length scales have to be considered as their relative magnitude determines the nature of the superconducting state and also the response to electromagnetic fields. The first length scale is the London penetration depth

$$\lambda_L = \left(\frac{mc^2}{4\pi Ne^2}\right)^{1/2} = \frac{c}{\omega_p} \tag{8}$$

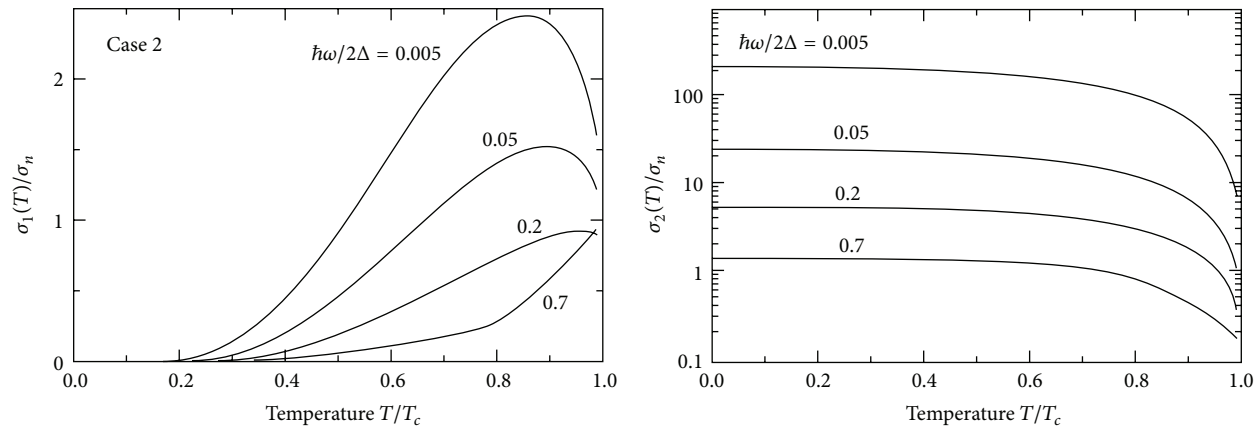

FIGURE 6: Temperature dependence of the conductivity of a superconductor at different frequencies ω with respect to the gap frequency $2\Delta/\hbar$. (a) For low frequencies the conductivity first rises as T decreases below T_c and exhibits a pronounced maximum before it drops to zero for $T \to 0$. This so-called coherence peak becomes smaller as the frequency increases; eventually $\sigma_1(\omega)/\sigma_n$ drops monotonously to zero. (b) The imaginary part $\sigma_2(\omega)/\sigma_n$ increases continuously with decreasing temperature. In the static limit, it resembles the development of the superconducting gap $\Delta(T)$ [46].

determined through the plasma frequency $\omega_p = (4\pi Ne^2/m)^{1/2}$ by the parameters of the metallic state, that is, the density of charge carriers N, the carrier mass m, and the electronic charge $-e$. The second length scale is the correlation length

$$\xi_0 = \frac{\hbar v_F}{\pi\Delta} \tag{9}$$

describing, crudely speaking, the spatial extension of the Cooper pairs. This is the length scale over which the wave function can be regarded as rigid and cannot respond to a spatially varying electromagnetic field. This parameter is determined through the energy gap Δ, which is linked to critical temperature by the coupling parameter $\alpha = 2\Delta/k_B T_c$. The third length scale is the mean free path of the uncondensed electrons

$$\ell = v_F \tau \tag{10}$$

set by the impurities and lattice imperfections at low temperatures; v_F is the Fermi velocity; τ is the time between two scattering events. For typical metals in the superconducting state, the three length scales are of the same order of magnitude, and, depending on the relative magnitude various types of superconductors are observed, these are referred to as the various limits. The local limit is where $\ell \ll \xi, \lambda$; more commonly it is referred to as the dirty limit defined by $\ell/\xi \to 0$. In the opposite, so-called clean limit $\ell/\xi \to \infty$, it is necessary to distinguish the following two cases: the Pippard or anomalous limit, defined by the inequality $\lambda \ll \xi, \ell$ (type I superconductor), and the London limit for which $\xi \ll \lambda, \ell$ (type II superconductor). Figure 7 summarizes the relation between these different length scales and the respective limiting cases.

The relative magnitude of the mean free path with respect to the coherence length has important consequences on the penetration depth, and this can be described using spectral weight arguments. The mean free path is given by $\ell \approx v_F\tau$, while for the coherence length we get $\xi \approx v_F/\Delta$ and consequently in the clean limit $1/\tau < \Delta/\hbar$, while $1/\tau > \Delta/\hbar$ is the so-called dirty limit. In the former case the width of the Drude response in the metallic state, just above T_c, is smaller than the frequency corresponding to the gap $2\Delta/\hbar$, and the opposite is true in the dirty limit.

The spectral weight associated with the excitations is conserved by going from the normal to the broken symmetry states. While we have to integrate the real part of the normal-state conductivity spectrum $\sigma_1^n(\omega)$, in the superconducting phase there are two contributions: one from the condensate of the Cooper pairs $\sigma_1^{\text{coll}}(\omega)$ and one from the single-particle excitations $\sigma_1^{\text{sp}}(\omega)$; thus

$$\int_{-\infty}^{\infty} \left[\sigma_1^{\text{coll}} + \sigma_1^{\text{sp}}\right] d\omega = \int_{-\infty}^{\infty} \sigma_1^n d\omega = \frac{\pi}{2}\frac{Ne^2}{m} \tag{11}$$

assuming that all the normal carriers condense. The arguments for superconductors were advanced by Ferrell et al. [25, 26] who noted that the area A which has been removed from the integral upon going through the superconducting transition

$$\int_{0+}^{\infty} \left[\sigma_1^n - \sigma_1^s\right] d\omega = A \tag{12}$$

is redistributed to give the spectral weight of the collective mode with $\sigma_1(\omega = 0) = A\delta\{\omega\}$. By comparison of the following expression with the Cooper pair response derived in (4):

$$\sigma_1(\omega) = \frac{c^2}{8\lambda_L^2}\delta\{\omega = 0\}, \tag{13}$$

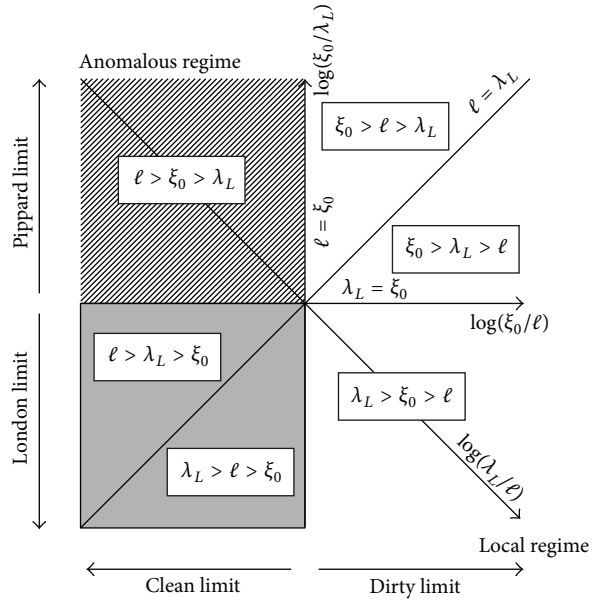

Figure 7: Schematic representation of the local, London, and Pippard limits in the parameter space given by the three length scales, the coherence length ξ_0, the London penetration depth λ_L, and the mean free path ℓ. In the local regime ℓ is smaller than the distance over which the electric field changes, $\ell < \xi(0) < \lambda$. When $\ell/\xi(0) \to 0$ the superconductor is in the so-called dirty limit. The opposite situation is in which $\ell/\xi(0) \to \infty$ is the clean limit, in which nonlocal effects are important, and we have to consider Pippard's treatment. This regime can be subdivided if we also consider the third parameter λ. The case $\xi(0) > \lambda$ is the Pippard or anomalous regime, which is the regime of type I superconductors; $\xi(0) < \lambda$ is the London regime, the regime of the type II superconductors [46].

we see that the missing spectral weight A is connected to the penetration depth λ by

$$\lambda = \frac{c}{\sqrt{8A}} \quad \text{or} \quad A = \frac{c^2}{8\lambda}. \tag{14}$$

This relation is expected to hold also at finite temperatures and also for various values of the mean free path and coherence length. In the limit of long relaxation time τ, that is, for $\hbar/\tau \ll \Delta$, all the Drude spectral weight of the normal carriers collapses in the collective mode, giving

$$\sigma_1(\omega = 0) = \frac{\pi N_s e^2}{2m}\delta\{\omega = 0\} \tag{15}$$

and through (4) leading to the London penetration depth λ_L. With increasing $1/\tau$, moving towards the dirty limit, the spectral weight is progressively reduced, resulting in an increase of the penetration depth. In the limit $1/\tau \gg 2\Delta/\hbar$, the missing spectral weight is approximately given by $A \approx \sigma_1(2\Delta/\hbar) = 2Ne^2\tau\Delta/\hbar m$ which can be written as

$$A = \frac{c^2}{2\pi}\frac{\tau\Delta}{\hbar}. \tag{16}$$

Then the relation between the area A and the penetration depth $\lambda(\ell)$—which now is mean free path dependent as $\ell = v_F\tau$—is given by $\lambda^2(\ell) = \lambda_L^2\hbar\pi/(4\tau\Delta)$, which leads to the approximate expression

$$\lambda(\ell) \approx \lambda_L\sqrt{\frac{\xi_0}{\ell}}. \tag{17}$$

3. Experimental Results

3.1. Coherence Peak. In order to determine the temperature dependence of the complex conductivity at frequencies well below the superconducting gap, Klein et al. [37] have performed precise measurements of the complex surface impedance of Nb using cavity perturbation methods [78–80]. A bulk Nb sample of 99.9% purity was used to replace the endplate of a 60 GHz cylindrical copper cavity. An abrupt drop of the bandwidth was observed upon cooling through the 9.3 K transition temperature. In Figure 8(a) the temperature dependence of the surface resistance R_s and surface reactance X_s normalized to the normal state value (defined as the value when the temperature of the sample is slightly above T_c, i.e., ~10 K): $R_n = (0.0538\,\Omega)/Z_0$ (where Z_0 is the free space impedance), corresponding to $\sigma_n(T = 10\,\text{K}) = 0.85 \cdot 10^6\,(\Omega\,\text{cm})^{-1}$. Below T_c, the surface resistance $R_s(T)$ drops rapidly with decreasing temperature, as shown in the logarithmic plot of Figure 8(a). The length scale for the surface reactance is determined by the skin depth in the normal state $\delta = 2270$ Å. $X_s(T)$ saturates at low temperatures, yielding a penetration depth $\lambda(0) = 440$ Å. Using the

measured values of R_s and X_s, the temperature dependence of the complex conductivity was evaluated and displayed in Figure 8(b). The coherence peak can be seen as a wide peak below T_c. The solid curves represent the Mattis-Bardeen results [(1) and (2)], while the dashed line corresponds to the Eliashberg theory for strong coupling [37].

Only recently, broadband microwave measurements on Al films succeeded to probe the coherence peak of a superconductor (as shown in Figure 2) both as a function of temperature and frequency. Steinberg et al. [29] employed a broadband microwave Corbino spectrometer [81] where basically a coaxial microwave line is terminated by the sample, in this case, a 550 Å aluminum film on a sapphire substrate. Using a vector network analyzer, the complex reflection coefficient is measured in the spectral range from 45 MHz to 60 GHz, allowing the calculation of the real and imaginary parts of the conductivity after also the calibration measurements have been performed with high precision. The method is most sensitive when the film impedance is close to the waveguide impedance of 50 Ω. For thicker or thinner films different geometries are possible [82]. The specimen is cooled down to 1.1 K and even lower temperatures are available [83]. Figure 9(a) shows data (taken at different frequencies on a film with thickness 500 Å and a room temperature resistivity of $8.7 \cdot 10^{-5}$ Ω cm) of the temperature dependence of the real part of the conductivity. σ_1 is governed by thermally excited charge carriers above and below the gap; their density of states diverges at the gap edge as depicted in Figure 3. Right below T_c, $\Delta(T)$ is small: both the thermal energy and the photon energy $\hbar\omega$ are sufficient to break up Cooper pairs. The imaginary part $\sigma_2(\omega)/\sigma_n$ displayed in the lower frame basically describes the temperature dependence of energy gap, in full agreement with (7).

In accord with theory, the coherence peak is seen as a maximum in $\sigma_1(T)$ at approximately $0.8T_c$ in the low-frequency limit; it becomes smaller with increasing frequency and shifts to higher temperatures in according to (6); this is clearly observed in Figure 9(a). Above 28 GHz [corresponding to $0.2 \cdot \Delta(0)$] the peak is completely suppressed, and for higher frequencies $\sigma_1(T)$ monotonously drops below T_c.

3.2. Energy Gap. In order to explore the energy gap in a superconductor the most straight-forward experiment is a transmission measurement through metallic films in the relevant frequency range around ω_g, and to vary the temperature from above to below T_c, as first has been done by Glover III and Tinkham on lead films in 1956 [10]. In Figure 10(a) the transmission through a NbN film at different temperatures as indicated normalized to the transmission in the metallic state just above $T_c = 13.5$ K [84]. With decreasing temperature a maximum in $\mathrm{Tr}_s/\mathrm{Tr}_n$ is observed that becomes more pronounced and shifts to higher frequencies. As sketched in Figure 1(b) it marks the superconducting energy gap 2Δ; in this case $2\Delta/hc = 35\,\mathrm{cm}^{-1}$.

The effect of the scattering rate on the transmission through superconducting NbN films has been explored experimentally [86] and analyzed on the basis of Leplae's theory [73] that describes strong-coupling materials. By reducing the film thickness from 100 to 20 nm, the critical temperature T_c is lowered from 17 to 14 K, but, more importantly, the energy gap $2\Delta(0)/hc$ is reduced from $52\,\mathrm{cm}^{-1}$ to $39\,\mathrm{cm}^{-1}$. Also the transmission maximum becomes significantly lower. Recently, it was shown [87, 88] that when the superconducting state is suppressed by a magnetic field, this transmission maximum broadens and shifts to lower temperatures. This is in agreement with the fact that the maximum in transmission corresponds to the energy gap. Using the transmission of $13.5\,\mathrm{cm}^{-1}$ gas laser the transmission through a 80 nm NbN film on a Si substrate was measured as a function of temperature for different external fields (Figure 11). With higher frequencies, the transmission peak first becomes more pronounced and shifts to lower temperatures; however, it eventually vanishes at $\omega_g \approx 2\Delta/\hbar$. When a magnetic field is applied parallel to the propagation direction (Faraday geometry), the electric field vector is perpendicular to the external magnetic field. For the Voigt geometry, the external field is chosen parallel to the electric field vector. The different behavior reflects the vortex dynamics in this constraint geometry determined by the thin superconducting film. The high-frequency response of type-II superconductors in the mixed state was extensively studied by Coffey and Clem [89, 90].

The absorption of electromagnetic radiation by a superconductor was directly investigated by measuring the temperature increase due to the deposited energy (bolometric absorption). A sputtered thin film of NbN on a silicon substrate (0.39 mm) was mounted at the bottom of a highly reflecting copper light cone, supported by four strands of 25 μm diameter gold wire of about 1.5 mm long. This gives the bolometer a thermal response time constant of about 30 ms at 10.8 K. The temperature is measured by a small doped silicon thermometer glued to the back of the silicon substrate. The resistance of this thermometer is exponentially decreasing with increasing temperature [85]. In Figure 10(b) the relative power absorption spectra are plotted for a 250 nm NbN superconducting film ($T_c = 13.3$ K) on a 0.39 mm silicon substrate. The curves are taken at 5.3 K and 10.8 K and each normalized to a normal state spectrum taken at $T = 14$ K. With decreasing frequency, the absorption increases and exhibits a maximum around the superconducting energy gap, before it rapidly drops to zero; the behavior is more pronounced for lower temperatures. On the same thin film, reflection measurements have been performed using Fourier-transform spectrometer with a resolution of $0.5\,\mathrm{cm}^{-1}$. Figure 10(c) shows the reflectivity of the NbN film on Si substrate above and below T_c. The reflectivity in the normal state is relatively low (due to the particular film thickness), making the superconductivity behavior very evident. While in the normal state at 15.5 K the reflectivity levels off around $R \approx 0.93$, a pronounced dip is observed in the superconducting state before the reflectivity rapidly rises to 1.0 ± 0.01 for frequencies below $40\,\mathrm{cm}^{-1}$, clearly indicating the superconducting gap frequency. In any case the high-resolution reflection spectra exhibit pronounced interference fringes due to multireflection within the Si substrate. In particular, one can see in the inset that the phase of the fringes at 5.3 K

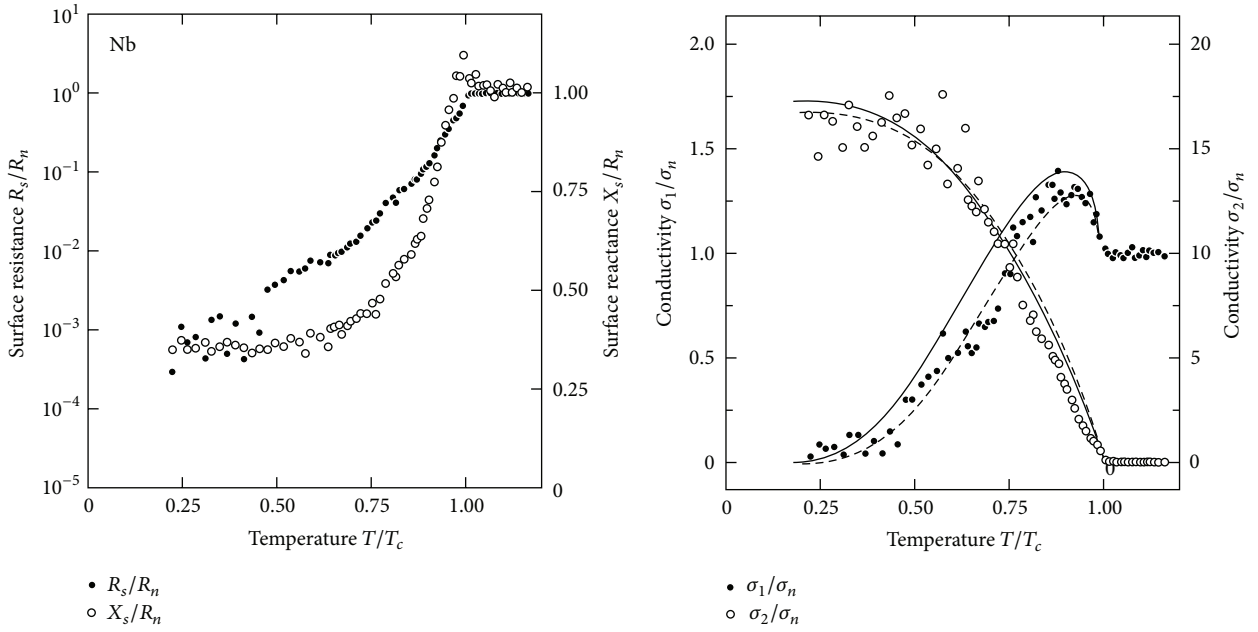

FIGURE 8: (a) Real component $R_s(T)$ (referring to the logarithmic scale on the left axis) and imaginary component $X_s(T)$ (right axis) of the surface impedance of niobium, normalized to the normal state surface resistance R_n measured at 60 GHz as a function of temperature. (b) Temperature dependence of the components of the conductivity $\sigma_1(T)$ and $\sigma_2(T)$ in niobium calculated from the results of the surface impedance shown in (a). Note the enhancement of $\sigma_1(T)$ just below $T_c = 9.2$ K. The full lines are calculated using the Mattis–Bardeen formalism [(1) and (2)] in the local limit, and the dashed lines follow from the Eliashberg theory of a strong coupling superconductor (after [37, 46]).

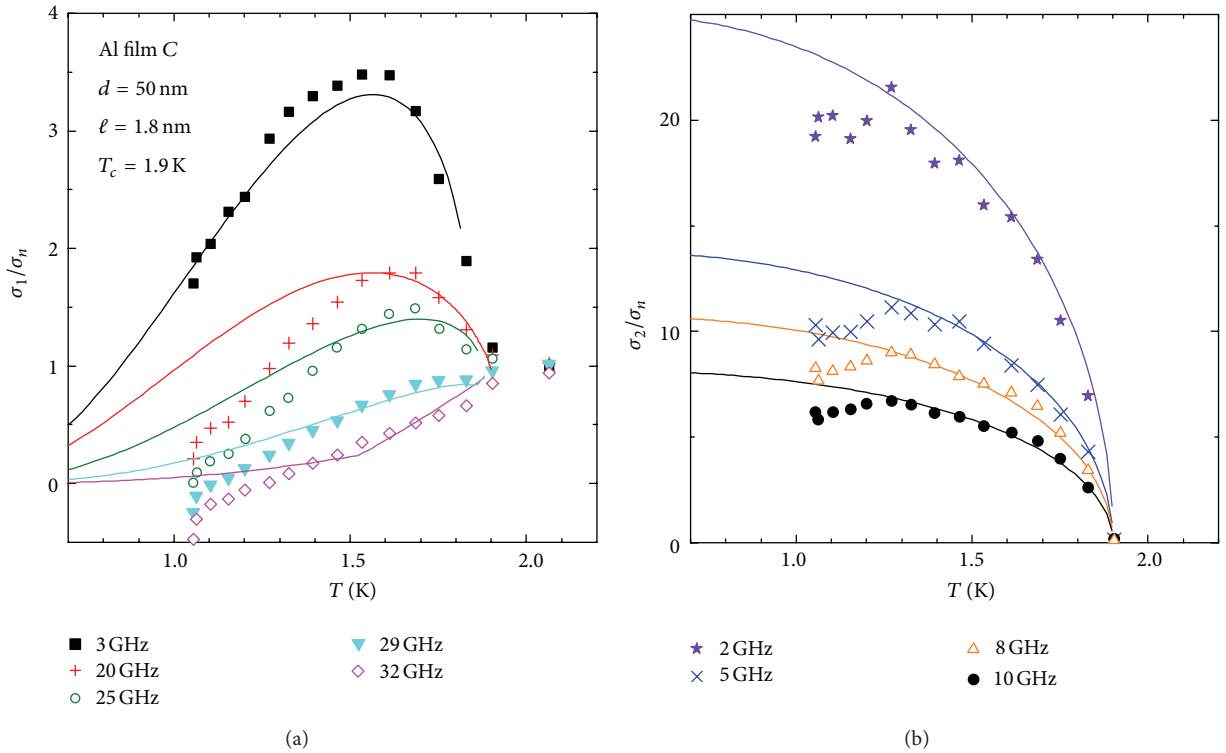

FIGURE 9: Temperature dependence of the (a) real and (b) imaginary parts of the conductivity of aluminum normalized to the normal state conductivity σ_n for selected frequencies. The solid lines are calculated by the BCS theory using $\ell/(\pi\xi) = 0.03$ [28].

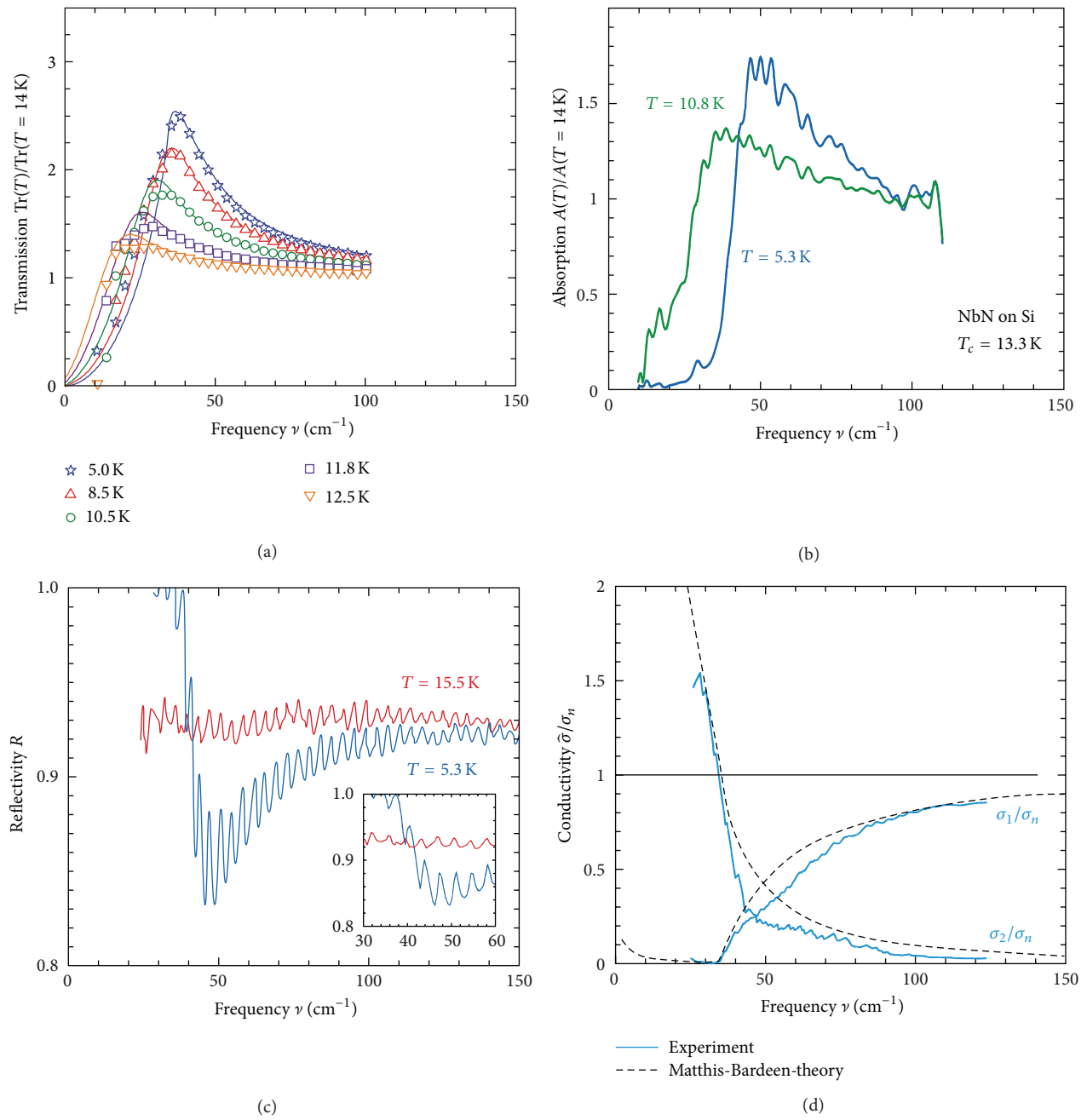

FIGURE 10: (a) Ratio of the infrared transmission through a NbN film in the superconducting state and the normal state for several temperatures; the critical temperature of this film is $T_c = 13.5$ K (after [84]). (b) The bolometric absorption spectra of a superconducting NbN film at different temperatures below $T_c = 13.3$ K ratioed with a 14 K spectrum above T_c. The curves have been scaled individually to agree at 110 cm^{-1} (for the purpose of comparison) and overall to give a 5.3 K spectrum, which equals 1.0 at large wave numbers. The resolution is 2 cm^{-1}. (c) Optical reflectivity of a 250 nm NbN film on silicon ($d = 0.39$ mm) above and below the superconducting transition temperature. The resolution was 0.5 cm^{-1} below 100 cm^{-1} and 2 cm^{-1} above. The inset gives the low-frequency part on a magnified scale in order to demonstrate the shift of the Fabry-Perot resonance pattern: At high frequencies the reflection maxima are in phase, but, for low frequency, the reflectivity in the superconducting state exhibits minima where maxima are observed for $T > T_c$. (d) Real and imaginary parts of the conductivity at $T = 5.3$ K normalized to the normal state value, as extracted from the reflection data shown above. The dashed lines correspond to the calculations based on Mattis-Bardeen theory, yielding an energy gap $2\Delta/hc = 34.5$ cm^{-1} (after [85]).

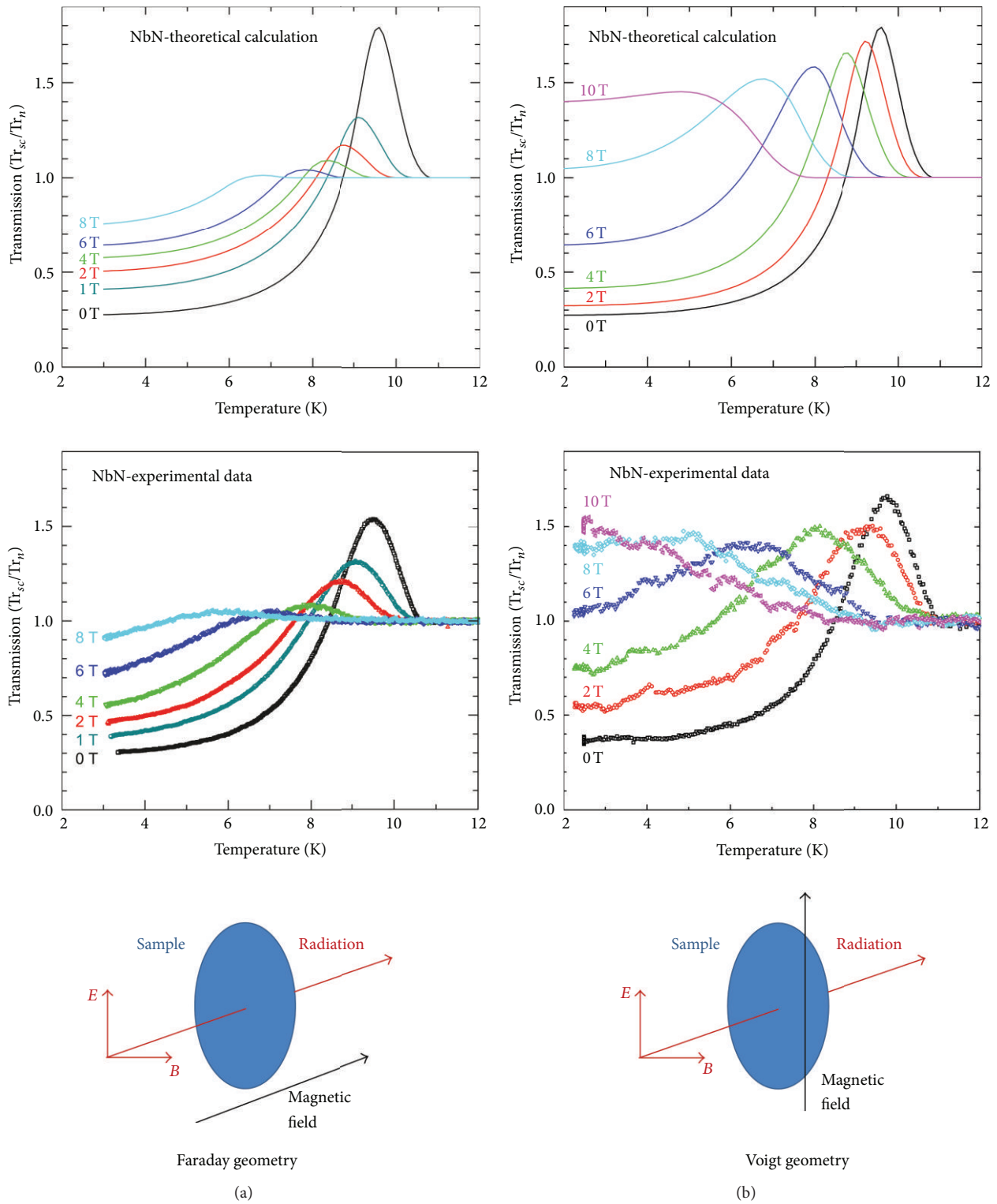

FIGURE 11: Temperature-dependent normal-incidence transmission of 13.5 cm^{-1} radiation through a 80 nm NbN film on a Si substrate of 0.25 mm thickness. The orientation is either in Faraday geometry ($B_0 \perp E$), shown in the left column, or in Voigt geometry ($B_0 \parallel E$) as shown in the right column. The calculations are done using a phenomenological effective medium approach (after [87]).

changes with respect to those at 15.5 K near 46 cm^{-1}. Above 46 cm^{-1} the fringes are in phase, while below they are 180° out of phase. From the lower panel (Figure 10(d)) we see that this is the frequency where the real and imaginary parts of the conductivities are equal at 5.3 K. The metallic reflection turns into a dielectric reflection, governed by the out-of-phase response of the Cooper pairs, leading to a sign change in the reflection coefficient. Using Fresnel's equations in order to describe the complete system of film and substrate, the Fabry-Perot pattern allows the calculation of the real and imaginary parts of the conductivity as displayed in Figure 10(c). No Kramers-Kronig transformation is used here, and thus no extrapolation or other model is required. The results agree very well with the theoretical predictions by Mattis and Bardeen [27], except slightly above ω_g. The superconducting gap is larger than expected from weak-coupling mean-field theory: $2\Delta(0)/k_BT_c = 3.9$; this is in agreement with the strong coupling nature of the Nb compounds.

While the previous experiments have been performed utilizing Fourier-transform spectrometers, Gorshunov et al. employed a THz spectrometer on the basis of tunable coherent monochromatic backward wave oscillators [93–95] to measure 115 Å thin NbN films on sapphire substrate [91, 92]. They demonstrated that for frequencies below 2Δ the error bars are too large to draw conclusions about the superconducting state and in-gap states, for instance. However, if the substrate is covered with a superconducting film on both sides (double-sided film), the Fabry-Perot resonances get much sharper (increase in quality factor) and the conductivity can be evaluated with a much larger precision, allowing even to observe the coherence peak right below the transition temperature. The raw data if the THz transmission are plotted in Figures 12(a) and 12(b) for single and double sided films; the corresponding conductivity spectra are plotted in panel (c) for two different frequencies close to and well below the superconducting gap 2Δ.

3.3. Complex Conductivity. Very similar results have been achieved by Nuss et al. [96] using THz time-domain spectroscopy. The amplitude transmitted through a thin Nb film ($T_c = 6.25$ K) is plotted in Figure 13 as a function of time. Both the amplitude and phase of the transients change as the film becomes superconducting. In accord with the observations of Glover III and Tinkham [10, 12] and others, the transmission in the superconducting state is higher than in the normal state. Since time-domain spectroscopy actually probes the electric field intensity and the shift in time, the real and imaginary parts of the conductivity can be calculated directly as plotted in Figure 13(b). The agreement with the BCS theory [27] shown by the dashed line is very good.

Alternatively a Mach-Zehnder interferometer allows one to measure both the change in transmission and phase shifts when the electromagnetic radiation passes through a metallic and superconducting film. This method was intensively explored by Gorshunov and collaborators [93–95]. Figure 14 displays the results of a transmission experiment [97] performed on a thin niobium film (thickness 150 Å) on a 0.45 mm thick sapphire substrate using a Mach-Zehnder interferometer. The substrate acts as a Fabry-Perot resonator due to multireflection leading to pronounced interference fringes in the spectra; this effect enhances the interaction of the radiation with the film considerably and thus improves the sensitivity and accuracy. In Figures 14(a) and 14(b) the transmission Tr_F and relative phase shifts ϕ/ν, respectively, through this composite sample are shown as a function of frequency. As the temperature decreases below the superconducting transition $T_c = 8.3$ K, the transmitted power and phase shifts are modified significantly. Since the properties of the dielectric substrate do not vary in this range of frequency and temperature, the changes observed are due to the electrodynamic properties of the superconductor [97]. When cooling from $T = 9$ to 6 K, the overall transmission increases for frequencies above 15 cm^{-1} while it drops for lower frequencies. The inset illustrates this behavior nicely. This corresponds to the theoretical predictions (Figure 1(b)) and previous observations. The maximum in the transmission corresponds to the superconducting energy gap 2Δ. Similar changes are observed in the relative phase shift (Figure 14(b)), where a strong decrease is found for $\omega < \omega_g$. The energy gap is evaluated to $2\Delta(0)/hc = 24\,cm^{-1}$. The data can be used to directly calculate the real and imaginary parts of the complex conductivity without using any model or assumption. In Figure 15 the real and imaginary parts of the conductivity of a Nb film are plotted as a function of frequency covering an extremely large range. Since the data are not normalized, the Drude roll-off becomes obvious above 100 cm^{-1}, placing the material into the dirty limit. In all cases it seems to be difficult to actually measure the zero-conductivity well below the gap for very low temperatures. In many cases some residual absorption seems to be present which can either be intrinsic due to some in-gap absorption, or due to inhomogeneities, impurities, surface effects, and so forth.

Thin films of NbN and TaN are perfectly suited for superconducting nanowire single-photon detectors [57, 59] which are built by thin and narrow superconducting stripes typically in a meander-like geometry. The device is driven with a dc bias current slightly below the critical current value. Absorption of a photon locally reduces the critical current below the applied dc bias current; consequently the superconducting state breaks down locally: this generates a normal-conducting spot (hot spot) and increases the resistance. The recovery time is in the picosecond range [63]. Since their performance in the far-infrared strongly depends on the optical properties of the device in this spectral range, the energy gap 2Δ, and the development of $\sigma_2(\omega)$, the information of THz and infrared investigations are highly desired. In particular it is important to study the influence of substrate, film thickness, processing parameters, structuring, and so forth. In Figure 16 the frequency dependence of the real and imaginary parts of the conductivity $\sigma_1(\omega)$ and $\sigma_2(\omega)$ is plotted for selected temperatures [72, 98]. The NbN film is deposited on a 10 mm × 10 mm R-plane-cut birefringent sapphire substrate using reactive dc-magnetron sputtering, which is a well-established and powerful way of film deposition with high demands concerning the performance of single-photon

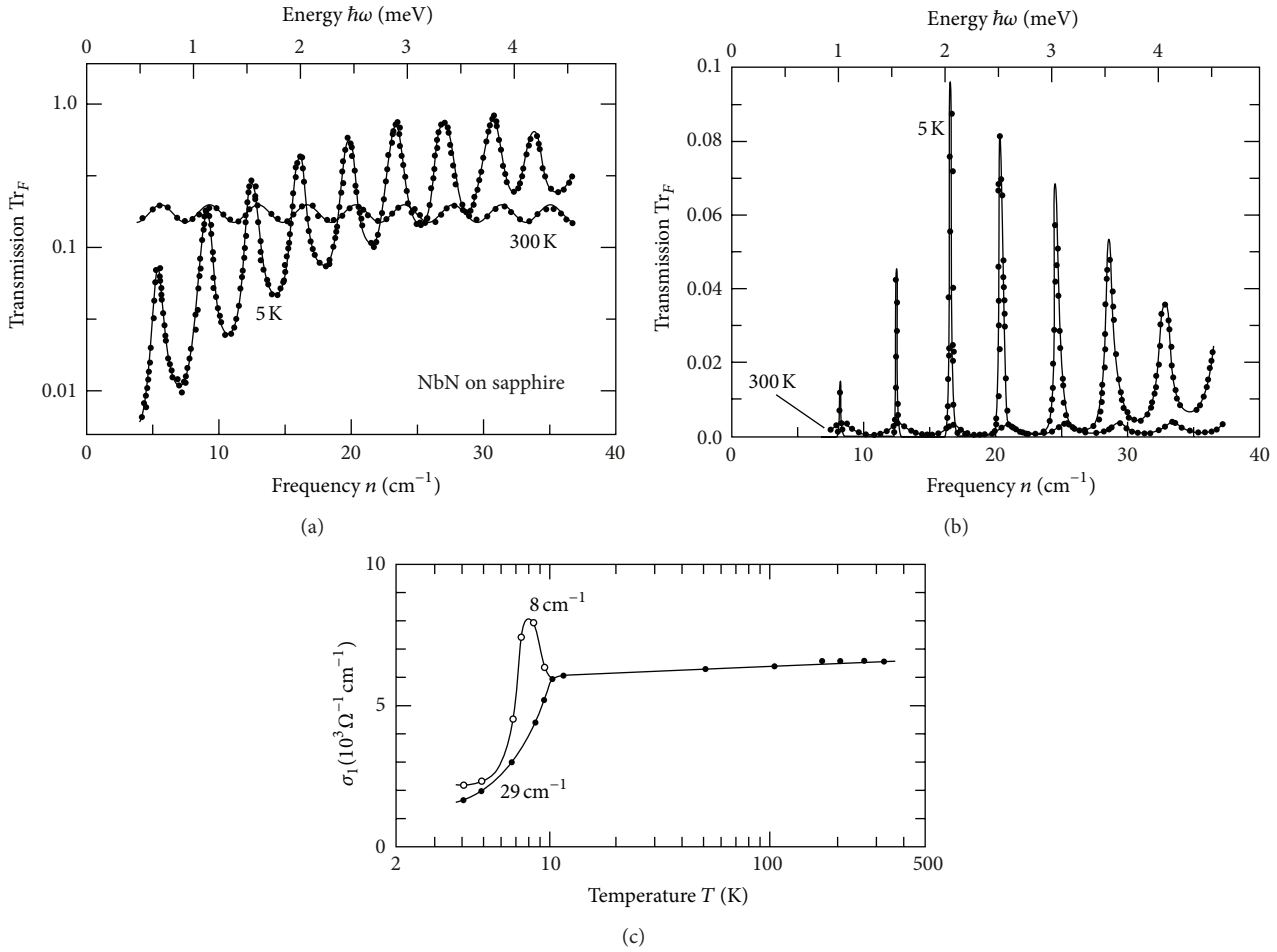

FIGURE 12: (a) Transmission spectra $\mathrm{Tr}_F(\nu)$ of an asymmetrical Fabry-Perot resonator, formed by a NbN film (d_2 = 115 Å) on a sapphire substrate (0.43 mm), measured at two temperatures above and below critical temperature $T_c \approx 12$ K. (b) Transmission spectra $\mathrm{Tr}_F(\nu)$ of a plane parallel sapphire plate (0.41 mm) covered with NbN films on both sides (d_2 = 250 Å and d_4 = 60 Å), again measured at 300 K and 5 K. The solid lines represent the theoretical fit. (c) For the latter case the temperature dependence of the optical conductivity $\sigma_1(T)$ of NbN film is calculated for two frequencies, 8 cm^{-1} and 29 cm^{-1} (after [91, 92]).

detectors [57, 58]. Typical films have a thickness of d = 39 to 47 Å. Since the thickness d is similar to the superconducting coherence length ξ and much smaller than the penetration depth λ, the films are considered ultrathin, that is, quasi-two dimensional, from the superconducting point of view. However, the electron mean free path ℓ is about one order of magnitude smaller than d, which justifies the 3D expressions used in the analysis and places the material in the dirty limit (Figure 7). Depending on the deposition current I_d while sputtering, the critical temperature is lowered in the case of NbN from 12.2 K (I_d = 100 mA) to 8.5 K (200 mA) [58, 59, 72, 98, 99]. The degree of disorder can be described by the Ioffe-Regel parameter $k_F\ell$, (with k_F the Fermi wave vector and ℓ the mean free path) ranging from 4.5 to 5.5; that is, in the present case these films are still weakly disordered.

Figure 17(a) displays the temperature dependent energy gap $2\Delta(T)$ of the sample with lowest disorder and highest T_c. Filled and open symbols refer to different main axes of the substrate and coincide within the range of error. Data for each main axis is fitted separately with the BCS expression. For $0.3T_c < T < 0.8T_c$ the measured energy gap is slightly above the BCS curve and for $0.8T_c < T < T_c$ below. Upon decreasing T_c, the energy gap (at 4.2 K) is also reduced from 4.5 to 3.3 meV; compare Figure 17(b). Consequently, $2\Delta(T)$ depends on the amount of disorder and is the greatest for low-disorder films. There are no traces or indications of superconductivity seen in the optical behavior of the normal state among the higher disordered samples as it is observed in tunneling studies [51]. At 4.2 K, $2\Delta(T)$ is reduced as T_c decreases (Figure 17(b)); ratio $2\Delta(0)/k_BT_c$ indicates that upon increasing disorder (decreasing T_c), the ratio $2\Delta(0)/k_BT_c$ which is first reduced from about 4.1, indicating strong-coupling superconductivity, exhibits a minimum and becomes larger again (about 4.5) towards the highest-disorder sample studied.

3.4. Dynamics. The question of how long it takes to break or recombine a Copper pair was considered from early

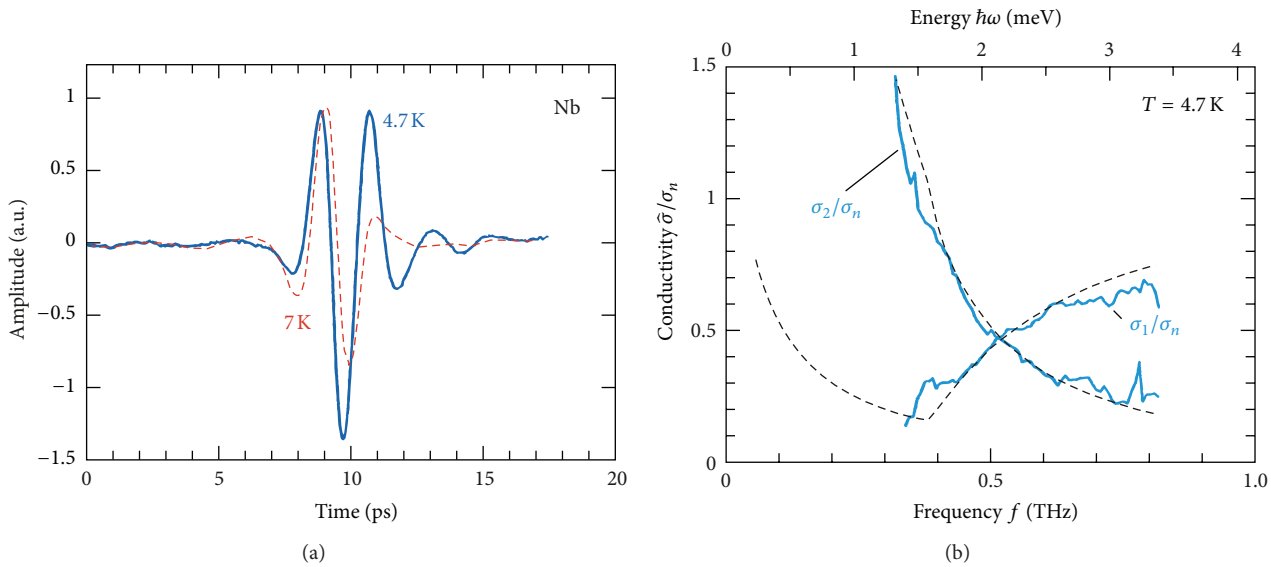

FIGURE 13: (a) THz transients transmitted through a thin niobium film (T_c = 6.25 K) on quartz in the normal state (dashed red line) and the superconducting state (solid blue line). (b) Real and imaginary parts of the normalized complex conductivity, $\sigma_1(\omega)$ and $\sigma_2(\omega)$, of Nb in the superconducting state evaluated from the above data (after [96]). The dashed black line indicates the predictions by the BCS theory using the Mattis-Bardeen equations (1) and (2). The energy gap is given by $2\Delta(0) = 3.8k_BT_c$.

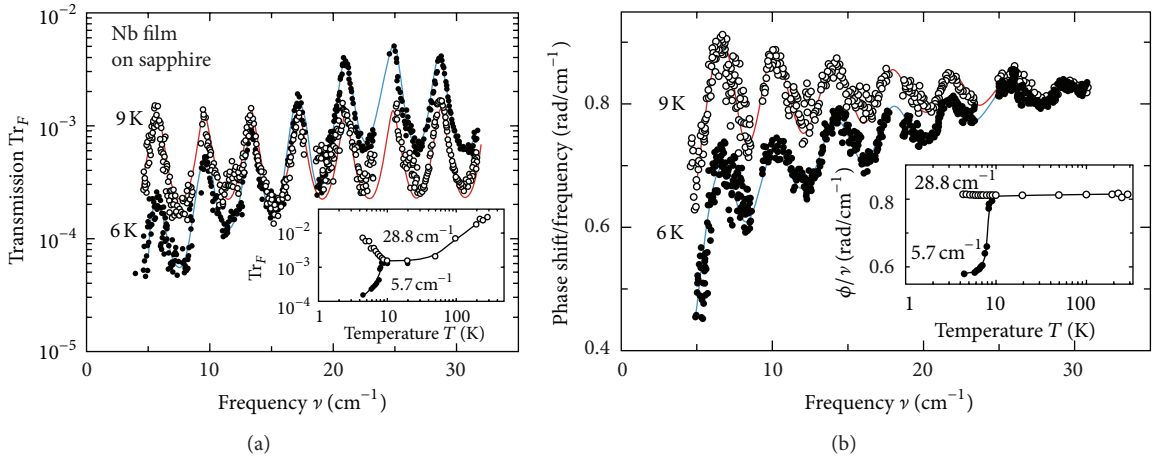

FIGURE 14: Raw data of transmission Tr(ω) and relative phase shift $\phi(\nu)/\nu$ spectra of the Nb film on the sapphire substrate. The critical temperature is T_c = 8.3 K. The phase shift is divided by the frequency $\nu = \omega/2\pi c$ for the better perception. The dots represent the measured values; the red lines for 9 K are the fits with the Drude model. The blue lines correspond to the fit using the Mattis-Bardeen equation. In the insets the temperature dependence of Tr and ϕ/ν is displayed for two particular frequencies corresponding to the first and last transmission maxima in measured spectral range (after [97]).

on [100, 101] and already linked to the possibility to use superconductors as quantum detectors in the microwave and THz range. Soon it became clear that not only radiative processes are important (emission of photons), but the emission of phonons dominates [102–104]. From early studies of the nonequilibrium conditions of superconductors [101] it became clear that the recombination of two quasiparticles to a Cooper pair requires the emission of phonons with energy above 2Δ. Rothwarf and Taylor [104] pointed out that reabsorption of high-energy phonons leads to the so-called phonon bottleneck: the recovery of the superconducting state is not governed by the bare recombination of two quasiparticles into the condensate; the return to equilibrium is rather limited by the phonon escape rate. It took some effort before the development of suitable light sources made the experimental investigations possible.

The first time Testardi [105] was able to break Cooper pairs by short laser light pulses (547 nm, 6–40 μs). The experiments are challenging due to the short penetration length of visible light into Pb metal and the heating of the sample. Federici et al. explored the dynamics of the optical response by looking at the photoinduced Cooper-pair breaking in lead

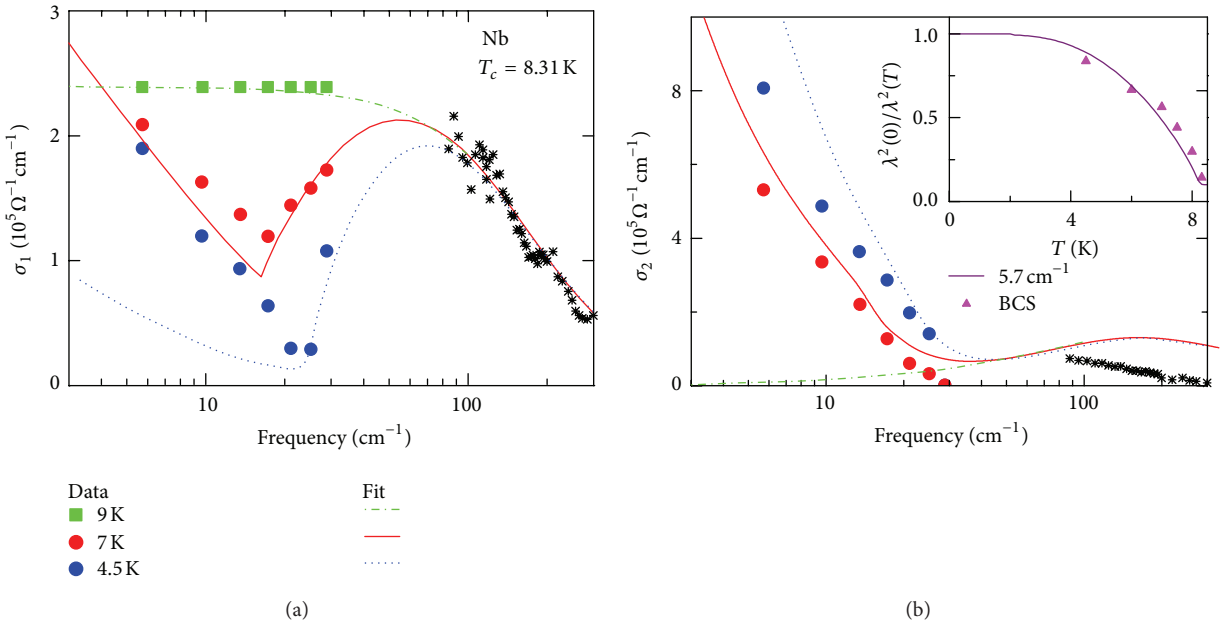

FIGURE 15: Frequency dependence of the real and imaginary parts of the conductivity, $\sigma_1(\omega)$ and $\sigma_2(\omega)$, in niobium at various temperatures T above and below the critical temperature T_c = 8.31 K. The transmission through a 150 Å thick film on sapphire was measured by a Mach-Zehnder interferometer; the stars were obtained by reflection measurements (after [97]). The lines are calculated using the theory of Mattis and Bardeen. The inset shows the temperature dependence of the penetration depth evaluated from the $\sigma_2(T)$ at the lowest frequency.

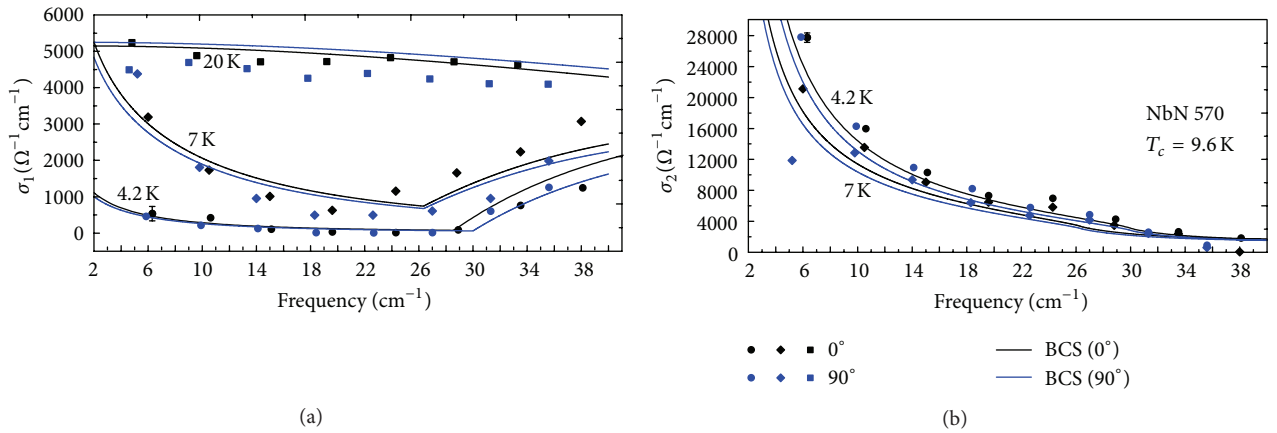

FIGURE 16: (a) Real part and (b) imaginary part of the complex conductivity versus frequency for 4.2 K (dots) and 7 K (diamonds) well below T_c = 9.6 K and 20 K (squares) in the normal state for both main axes of a NbN film. Solid black and blue lines are predictions calculated directly from raw data fits for both axes individually. The kink in σ_1 signaling the energy gap is resolved clearly. The error bar shown is representative for all data (after [98]).

[106]. 100 fs light pulses (630 nm, 1 μJ/cm^2) lead to an abrupt decrease of the transmission maximum within about 1 ps; it takes several nanoseconds before the superconducting state is recovered. This implies that the superconducting gap closes in less than one picosecond after the optical excitation. Kaindl et al. showed [107] that the imaginary part of the optical conductivity in NbN films abruptly changes and then relaxes in an exponential way (Figure 18(c)). The recovery time τ = 580 ps does not depend on the on intensity A_0 of the light pulse.

A more detailed picture is drawn by Demsar and collaborators who succeeded to perform a detailed study on the superconducting state relaxation phenomena in NbN films: both the Cooper-pair breaking and the recovery of the superconducting state depend on the temperature and energy density [108]. In Figure 18(d) the temporal evolution of the superconducting gap is shown after the sample is excited by a femtosecond pulse. The photoinduced change of the gap $\delta\Delta$ (normalized to the equilibrium energy gap at zero temperature) is plotted in Figure 19(a) for various laser

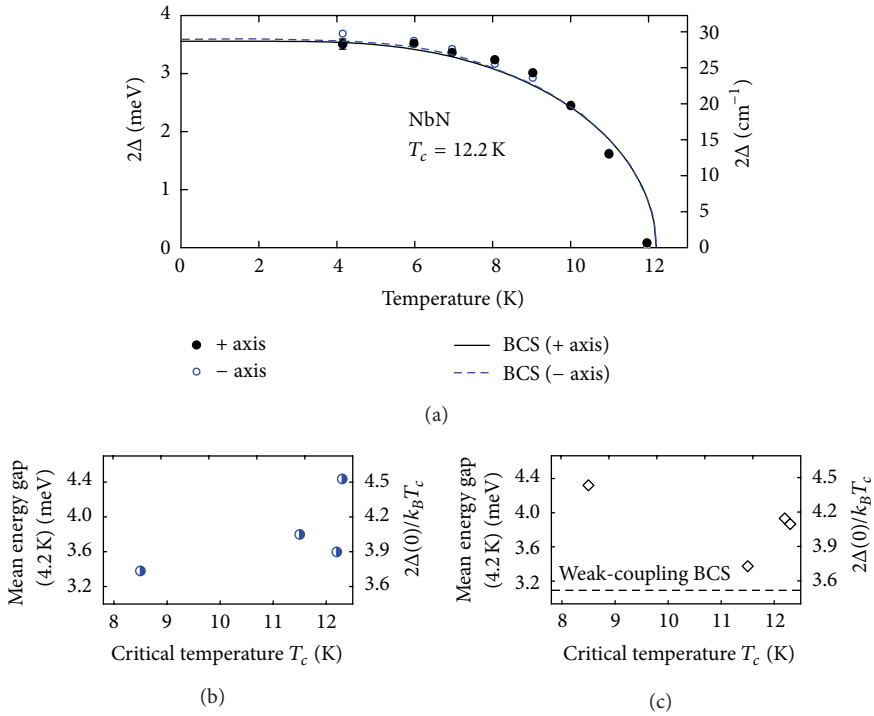

Figure 17: (a) Energy gap 2Δ versus temperature of a NbN sample for both main axes of the substrate. Solid lines are the fits according to BCS theory. Results on both main axes yield very similar values of $2\Delta(T)$. The error bar shown is representative for all data. (b) 2Δ at 4.2 K and (c) ratios $2\Delta(0)/k_BT_c$ versus T_c of several NbN films deposited with different parameters, yielding different transition temperatures (after [72]).

intensities. It can be seen that both the Cooper-pair breaking and the recovery of superconductivity depend on intensity A. The long timescale of the Cooper pair breaking implies that photoexcited hot electrons and holes create a high density of high-frequency phonons, which subsequently break Cooper pairs; this process reaches some equilibrium between quasiparticle population and high-frequency phonon population [108]. It is seen from Figure 19(b) that the maximum induced change first increases linearly with excitation intensity (note the logarithmic abscissa) but then saturates when superconductivity is suppressed: $\delta\Delta/\Delta_0 = 1 - \exp\{-A/A_{\text{sat}}\}$, where the temperature dependence of $A_{\text{sat}}(T)$, plotted in the inset, basically follows the superconducting density $\Delta^2(T)$. The superconducting recovery time τ_{rec} depends on temperature T and on intensity A, as shown in Figure 19(c). These findings support the phenomenological model of Rothwarf and Taylor [104] on the phonon bottleneck.

Matsunaga and Shimano [109] investigated the nonlinear dynamics of superconducting state in a NbN film by using intense THz pulses to pump the system which is then probed by time-domain spectroscopy in the same frequency range. After the intense pulse, superconductivity is rapidly switched off with the duration of the THz pulse. In contrast to the previous experiments with visible or infrared pump lasers, the THz pulse resonantly excites the low-energy quasiparticles without the process of phonon emission from hot electrons. The rapid time evolution after the THz pulse is basically independent of intensity implying direct photoinjection of quasiparticles. Figure 20 shows the conductivity spectra obtained at 20 ps after the pump with various intensities. With increasing pump intensity $\sigma_1(\omega)$ below the gap energy significantly increases and exceeds the normal state value (dashed line). At the gap energy of approximately 5 meV the conductivity $\sigma_1(\omega)$ remains always below the metallic behavior. This cannot be explained by the increase of the effective temperature and implies a high density of quasiparticles. For their analysis they apply an effective medium approach of superconducting and normal state phases. The conclusion is a spatially inhomogeneous suppression of the superconducting state on a length scale of 1 μm [110, 111].

4. Outlook

The effect of disorder on superconductivity is an ongoing intriguing topic of research that has puzzled physicists for decades. It was argued by Anderson in a seminal paper [112] in 1959 that s-wave superconductivity is not affected by the presence of mild nonmagnetic disorder, persisting even in polycrystalline or amorphous materials. Experimentally, however, it was found that superconductivity can be destroyed by a sufficiently large degree of disorder [113–118]. Once superconductivity is destroyed, the system undergoes a transition to an insulating state in what has been named the superconductor-insulator transition (SIT).

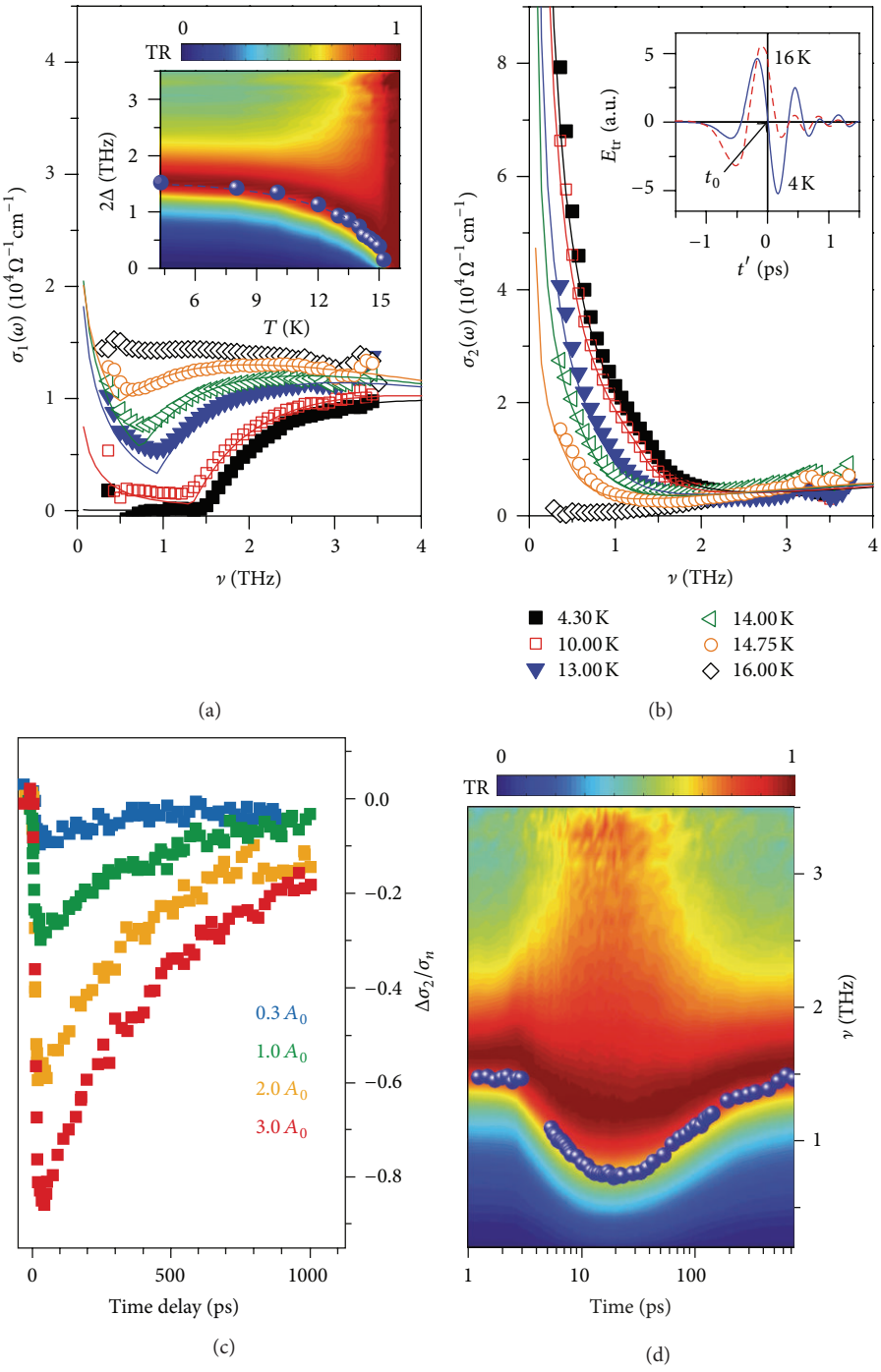

FIGURE 18: Temperature-dependence of the (a) real and (b) imaginary parts of the conductivity spectra obtained on a 15 nm NbN film on MgO substrate (T_c = 15.4 K). The solid lines are fits with the Mattis-Bardeen equations [27, 28]. The inset of panel (a) shows the temperature dependence of the energy gap 2Δ, extracted from fits to $\sigma(\omega)$ (symbols) overlaying the normalized transmissivity ratio, TR. The BCS temperature dependence of Δ is shown by the dashed line. The inset to panel (b) displays the transmitted THz transients through the NbN film below and above T_c; the arrow denotes the time $t' = t_0$ with maximum change in the transmitted electric field (after [108]). (c) The recovery of the imaginary part of the superconducting conductivity for different intensities can be described by a single exponential dependence with τ = 580 ps [107]. (d) Time evolution of normalized transmissivity ratio (TR), recorded at A = 22 mJ/cm^3, together with $\Delta(t)$ extracted from $\sigma_1(\omega, t_d)$ fit with the BCS theory [27, 28] (after [108]).

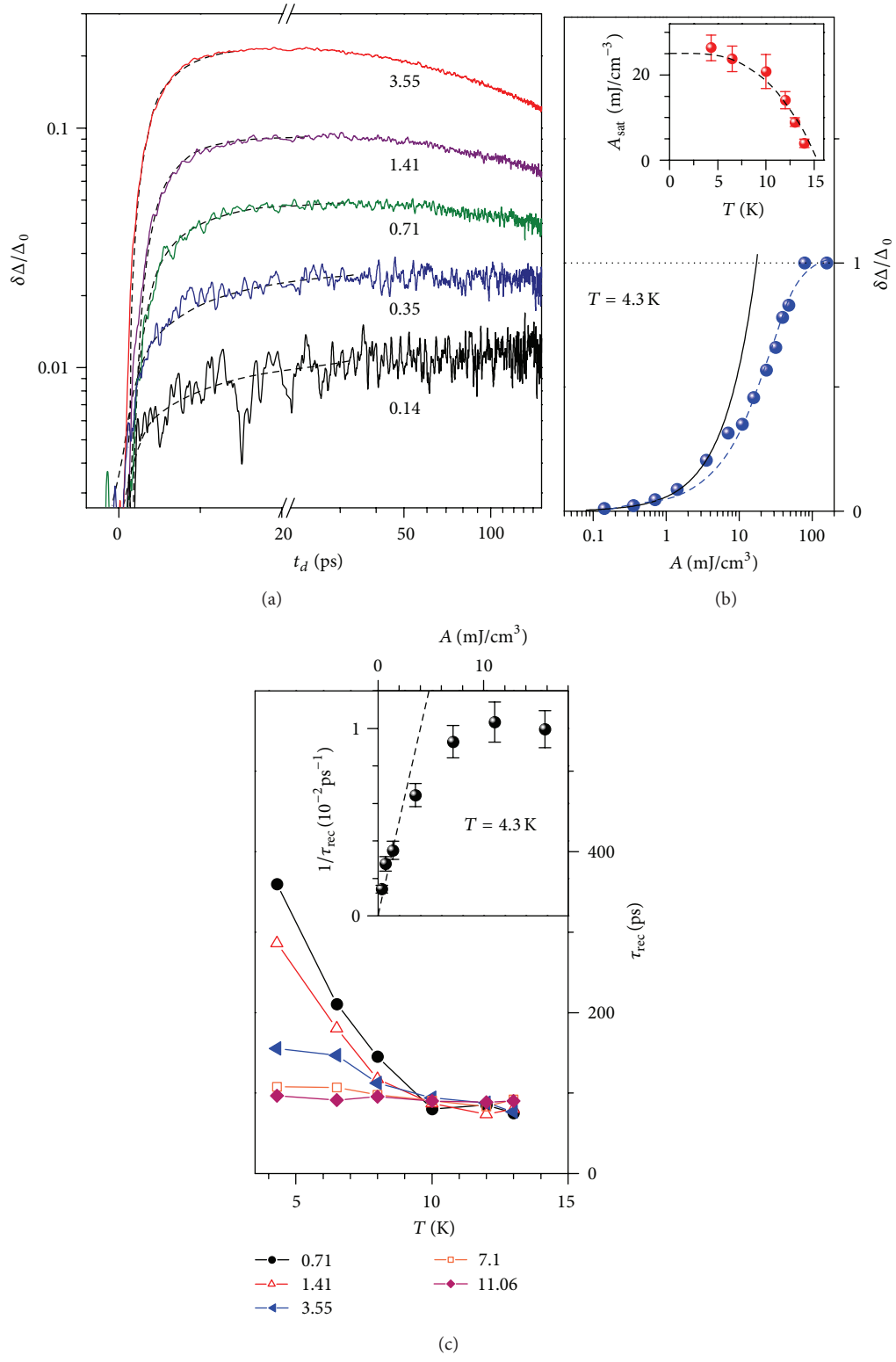

FIGURE 19: (a) The relative change in gap, $\delta\Delta/\Delta_0$ recorded at 4.3 K for various intensities A in mJ/cm^3. The dashed lines are fits to the data with (1). (b) The dependence of $\delta\Delta/\Delta_0$ on intensity A at 4.3 K. The dashed line is a fit to the simple saturation model; the solid line is the linear fit. Inset: the temperature dependence of the saturation energy density, A_{sat}, compared to the T-dependence of Δ^2 (dashed line). Panel (c) shows the T-dependence of the superconducting recovery time, τ_{rec}, for several intensities A (in mJ/cm ^{3}). Inset: $\tau_{rec}^{-1}(A)$ recorded at 4.3 K. For low intensities A the relaxation rate increases linearly with A (dashed line) (after [108]).

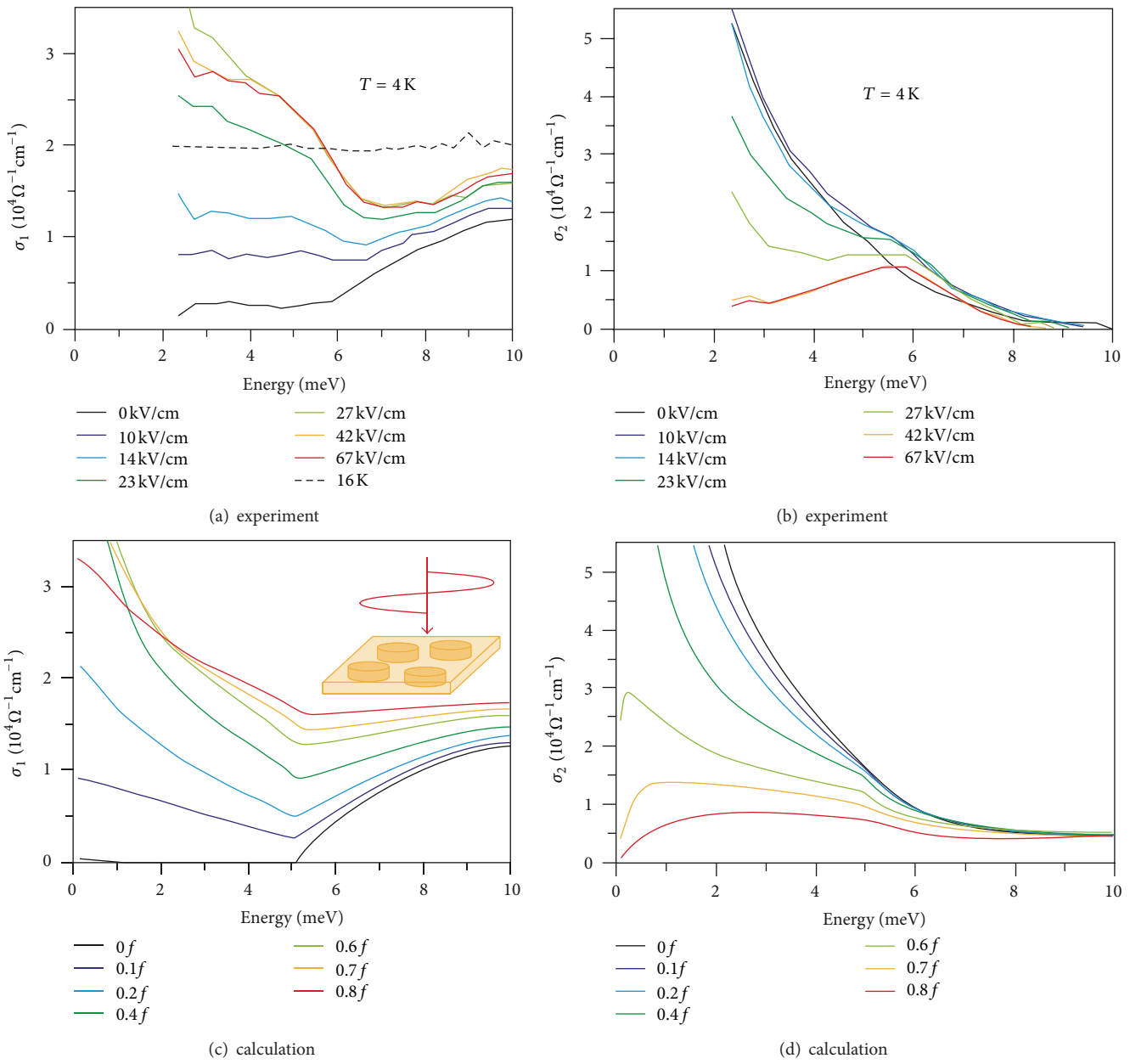

FIGURE 20: The spectra of the (a) real and (b) imaginary parts of the optical conductivity for various THz excitation intensities at 4 K. For reference, $\sigma_1(\omega)$ in the normal metal state at 16 K is plotted as a dotted line. Panel (c) and (d) exhibit the calculated real and imaginary parts of the optical conductivity spectra, respectively, using an effective medium approach. The inset is a schematic image of the inhomogeneously suppressed superconductivity (after [109]).

Interest in this field has been revived recently with the experimental observations of a number of dramatic features near the superconductor-insulator transition in InO, TiN and NbN, such as nonmonotonic temperature dependence of the resistivity, simple activated temperature dependence on the insulating side, large peak in the magnetoresistance, peculiar I-V characteristics, and existence of an energy gap at temperatures above T_c [119–130]. Another reason for renewed interest in this field is that the superconductor-insulator transition may be a very basic realization of a quantum phase transition, that is, a phase transition which occurs at $T = 0$ as a function of some nonthermal parameters (pressure, doping, magnetic field, etc.) and is driven by quantum instead of thermal fluctuations.

The nature of the superconductor-insulator transition and especially that of the insulating phase is still under debate. Recently several indications for the presence of superconductivity in the insulating state have been reported [131–133], and a number of possible explanations have been put forward. One suggestion relates the phenomena to the inhomogeneous nature of the system under study [134, 135]; near the superconductor-insulator transition on both sides

of the transition the system is composed of regions of superconducting material embedded in an insulating matrix. In this picture, the transition occurs when the isolated superconducting islands are able to Josephson-couple and allow the many-body wave function to percolate throughout the entire system. There are basic arguments [136, 137] and theoretical considerations [138, 139] that actually anticipate that inherent inhomogeneity has to occur near the superconductor-insulator transition even when the system is structurally uniform and compatible with the underlying disorder (which, near the SIT of a typical superconductor, is fairly strong). Therefore, some inhomogeneity is expected to be present near the superconductor-insulator transition in all systems where the transition temperature does not drop to zero before a substantial disorder has set in (which in 2D is equivalent to the SIT occurring when the sheet resistance $R_\square$ is of the order of the quantum resistance $\hbar/4e^2$).

There are quite a few systems that seem to exhibit transport properties that are consistent with this expectation. An example is the situation in amorphous InO films, one of the systems that showed the peculiar features alluded above. Structural study reveals morphological inhomogeneities on scales of order 100 Å. Transport studies, however, exposed scale dependences up to few microns [136, 137]. Another candidate is films of NbN that exhibit higher T_c and thus are suitable for optical experiments in the THz range.

A second picture invokes the existence of uncorrelated preformed electron pairs which do not constitute a condensate [129, 130, 140, 141] but are characterized by an energy gap that is associated with the pair binding energy. Other models adapt concepts from both pictures [142] and suggest that above T_c and on the insulating site the film is composed of small superconducting islands that are uncorrelated and are too small to sustain bulk superconductivity. Hence, the situation is unclear, and further experimental information is required.

Acknowledgments

The authours thank A. Frydman, B. Gorshunov, E. Heinze, U. Pracht, M. Scheffler, and D. Sherman for the fruitful collaboration and useful discussions. The work was supported by the Deutsche Forschungsgemeinschaft (DFG).

References

[1] F. London, *Superfluids*, vol. 1 of *Macroscopic Theory of Superconductivity*, John Wiley & Sons, New York, NY, USA, 1950.

[2] J. Bardeen, "Theory of the Meissner effect in superconductors," *Physical Review*, vol. 97, no. 6, pp. 1724–1725, 1955.

[3] J. Bardeen, "Theory of Supercondgctivity," in *Handbuch der Physik*, vol. 15, pp. 274–369, Springer, Berlin, Germany, 1956.

[4] H. Welker, "Supraleitung und magnetische Austauschwechselwirkung," *Zeitschrift für Physik*, vol. 114, no. 9-10, pp. 525–551, 1939.

[5] L. N. Cooper, "Bound electron pairs in a degenerate fermi gas," *Physical Review*, vol. 104, no. 4, pp. 1189–1190, 1956.

[6] J. Bardeen, L. N. Cooper, and J. R. Schrieffer, "Theory of superconductivity," *Physical Review*, vol. 108, no. 5, pp. 1175–1204, 1957.

[7] L. C. Hebel and C. P. Slichter, "Nuclear relaxation in superconducting aluminum," *Physical Review*, vol. 107, no. 3, p. 901, 1957.

[8] L. C. Hebel and C. P. Slichter, "Nuclear spin relaxation in normal and superconducting aluminum," *Physical Review*, vol. 113, no. 6, pp. 1504–1519, 1959.

[9] R. W. Morse and H. V. Bohm, "Superconducting energy gap from ultrasonic attenuation measurements," *Physical Review*, vol. 108, no. 4, pp. 1094–1096, 1957.

[10] R. E. Glover III and M. Tinkham, "Transmission of superconducting films at millimeter-microwave and far infrared frequencies," *Physical Review*, vol. 104, no. 3, pp. 844–845, 1956.

[11] M. Tinkham, "Energy gap interpretation of experiments on infrared transmission through superconducting films," *Physical Review*, vol. 104, no. 3, pp. 845–846, 1956.

[12] R. E. Glover III and M. Tinkham, "Conductivity of superconducting films for photon energies between 0.3 and 40kTc," *Physical Review*, vol. 108, no. 2, pp. 243–256, 1957.

[13] M. J. Buckingham, "Very high frequency absorption in superconductors," *Physical Review*, vol. 101, no. 4, pp. 1431–1432, 1956.

[14] G. S. Blevins, W. Gordy, and W. M. Fairbank, "Superconductivity at millimeter wave frequencies," *Physical Review*, vol. 100, no. 4, pp. 1215–1216, 1955.

[15] M. Tinkham and R. E. Glover III, "Superconducting energy gap inferences from thin-film transmission data," *Physical Review*, vol. 110, no. 3, pp. 778–779, 1958.

[16] A. T. Forrester, "Superconducting energy gap inferences from thin-film transmission data," *Physical Review*, vol. 110, no. 3, pp. 776–778, 1958.

[17] M. A. Biondi, A. T. Forrester, M. P. Garfunkel, and C. B. Satterthwaite, "Experimental evidence for an energy gap in superconductors," *Reviews of Modern Physics*, vol. 30, no. 4, pp. 1109–1136, 1958.

[18] M. A. Biondi, M. P. Garfunkel, and A. O. McCoubrey, "Millimeter wave absorption in superconducting aluminum," *Physical Review*, vol. 101, no. 4, pp. 1427–1429, 1956.

[19] M. A. Biondi, M. P. Garfunkel, and A. O. McCoubrey, "Microwave measurements of the energy gap in superconducting aluminum," *Physical Review*, vol. 108, no. 2, pp. 495–497, 1957.

[20] M. A. Biondi, A. T. Forrester, and M. P. Garfunkel, "Millimeter wave studies of superconducting tin," *Physical Review*, vol. 108, no. 2, pp. 497–498, 1957.

[21] M. A. Biondi and M. P. Garfunkel, "Measurement of the temperature variation of the energy gap in superconducting aluminum," *Physical Review Letters*, vol. 2, no. 4, pp. 143–145, 1959.

[22] M. A. Biondi and M. P. Garfunkel, "Millimeter wave absorption in superconducting aluminum. I. Temperature dependence of the energy gap," *Physical Review*, vol. 116, no. 4, pp. 853–861, 1959.

[23] M. A. Biondi and M. P. Garfunkel, "Millimeter wave absorption in superconducting aluminum. II. Calculation of the skin depth," *Physical Review*, vol. 116, no. 4, pp. 862–867, 1959.

[24] M. Tinkham, "Absorption of electromagnetic radiation in superconductors," *Physica*, vol. 24, supplement 1, pp. S35–S41, 1958.

[25] R. A. Ferrell and R. E. Glover III, "Conductivity of superconducting films: a sum rule," *Physical Review*, vol. 109, no. 4, pp. 1398–1399, 1958.

[26] M. Tinkham and R. A. Ferrell, "Determination of the superconducting skin depth from the energy gap and sum rule," *Physical Review Letters*, vol. 2, no. 8, pp. 331–333, 1959.

[27] D. C. Mattis and J. Bardeen, "Theory of the anomalous skin effect in normal and superconducting metals," *Physical Review*, vol. 111, no. 2, pp. 412–417, 1958.

[28] W. Zimmermann, E. H. Brandt, M. Bauer, E. Seider, and L. Genzel, "Optical conductivity of BCS superconductors with arbitrary purity," *Physica C*, vol. 183, no. 1–3, pp. 99–104, 1991.

[29] K. Steinberg, M. Scheffler, and M. Dressel, "Quasiparticle response of superconducting aluminum to electromagnetic radiation," *Physical Review B*, vol. 77, no. 21, Article ID 214517, 2008.

[30] D. M. Ginsberg, P. L. Richards, and M. Tinkham, "Apparent structure on the far infrared energy gap in superconducting lead and mercury," *Physical Review Letters*, vol. 3, no. 7, pp. 337–338, 1959.

[31] D. M. Ginsberg and M. Tinkham, "Far infrared transmission through superconducting films," *Physical Review*, vol. 118, no. 4, pp. 990–1000, 1960.

[32] P. L. Richards and M. Tinkham, "Far-infrared energy gap measurements in bulk superconducting in, Sn, Hg, Ta, V, Pb, and Nb," *Physical Review*, vol. 119, no. 2, pp. 575–590, 1960.

[33] L. H. Palmer and M. Tinkham, "Far-infrared absorption in thin superconducting lead films," *Physical Review*, vol. 165, no. 2, pp. 588–595, 1968.

[34] M. Tinkham, "The electromagnetic properties of superconductors," *Reviews of Modern Physics*, vol. 46, no. 4, pp. 587–596, 1974.

[35] P. Wyder, "Far-infrared and superconductivity," *Infrared Physics*, vol. 16, no. 1-2, pp. 243–251, 1976.

[36] K. Holczer, O. Klein, and G. Grüner, "Observation of the conductivity coherence peak in superconducting Pb," *Solid State Communications*, vol. 78, no. 10, pp. 875–877, 1991.

[37] O. Klein, E. J. Nicol, K. Holczer, and G. Grüner, "Conductivity coherence factors in the conventional superconductors Nb and Pb," *Physical Review B*, vol. 50, no. 9, pp. 6307–6316, 1994.

[38] A. B. Pippard, "Metallic conduction at high frequencies and low temperatures," *Advances in Electronics and Electron Physics*, vol. 6, pp. 1–45, 1954.

[39] A. B. Pippard, "The anomalous skin effect in anisotropic metals," *Proceedings of the Royal Society of London A*, vol. 224, no. 1157, pp. 273–282, 1954.

[40] J. R. Waldram, "Surface impedance of superconductors," *Advances in Physics*, vol. 13, no. 49, pp. 1–88, 1964.

[41] M. Tinkham, *Introduction to Superconductivity*, Mc-Graw Hill, New York, NY, USA, 1st edition, 1975.

[42] M. Tinkham, *Introduction to Superconductivity*, Mc-Graw Hill, New York, NY, USA, 2nd edition, 1996.

[43] M. Tinkham, *Introduction to Superconductivity*, Dover Publication, Mineola, NY, USA, 2nd edition, 2004.

[44] G. Rickayzen, *Theory of Superconductivity*, Interscience Publishers, New York, NY, USA, 1965.

[45] R. D. Parks, Ed., *Superconductivity, Vol. I and II*, Marcel Dekker, New York, NY, USA, 1969.

[46] M. Dressel and G. Grüner, *Electrodynamics of Solids*, Cambridge University Press, Cambridge, UK, 2002.

[47] D. N. Basov, R. D. Averitt, D. van der Marel, M. Dressel, and K. Haule, "Electrodynamics of correlated electron materials," *Reviews of Modern Physics*, vol. 83, no. 2, pp. 471–541, 2011.

[48] D. Sherman, G. Kopnov, D. Shahar, and A. Frydman, "Measurement of a superconducting energy gap in a homogeneously amorphous insulator," *Physical Review Letters*, vol. 108, no. 17, Article ID 177006, 2012.

[49] B. Sacépé, C. Chapelier, T. I. Baturina, V. M. Vinokur, M. R. Baklanov, and M. Sanquer, "Pseudogap in a thin film of a conventional superconductor," *Nature Communications*, vol. 1, no. 9, article 140, 2010.

[50] Y. Mizukami, H. Shishido, T. Shibauchi et al., "Extremely strong-coupling superconductivity in artificial two-dimensional Kondo lattices," *Nature Physics*, vol. 7, no. 11, pp. 849–853, 2011.

[51] S. P. Chockalingam, M. Chand, A. Kamlapure et al., "Tunneling studies in a homogeneously disordered s-wave superconductor: NbN," *Physical Review B*, vol. 79, no. 9, Article ID 094509, 2009.

[52] T. Timusk and B. Statt, "The pseudogap in high-temperature superconductors: an experimental survey," *Reports on Progress in Physics*, vol. 62, no. 1, pp. 61–122, 1999.

[53] N. D. Basov and T. Timusk, "Electrodynamics of high—T_c superconductors," *Reviews of Modern Physics*, vol. 77, no. 2, pp. 721–729, 2005.

[54] U. S. Pracht, M. Scheffler, M. Dressel, D. F. Kalok, C. Strunk, and T. I. Baturina, "Direct observation of the superconducting gap in a thin film of titanium nitride using terahertz spectroscopy," *Physical Review B*, vol. 86, no. 18, Article ID 184503, 2012.

[55] E. F. C. Driessen, P. C. J. J. Coumou, R. R. Tromp, P. J. de Visser, and T. M. Klapwijk, "Strongly disordered tin and nbtin s-wave superconductors probed by microwave electrodynamics," *Physical Review Letters*, vol. 109, no. 10, Article ID 107003, 2012.

[56] M. R. Vissers, M. P. Weides, J. S. Kline, M. Sandberg, and D. P. Pappas, "Identifying capacitive and inductive loss in lumped element superconducting hybrid titanium nitride/aluminum resonators," *Applied Physics Letters*, vol. 101, Article ID 022601, 2012.

[57] D. Henrich, S. Dörner, M. Hofherr et al., "Broadening of hotspot response spectrum of superconducting NbN nanowire singlephoton detector with reduced nitrogen content," *Journal of Applied Physics*, vol. 112, no. 7, Article ID 074511, 2012.

[58] K. Il'in, M. Hofherr, D. Rall et al., "Ultra-thin TaN films for superconducting nanowire single-photon detectors," *Journal of Low Temperature Physics*, vol. 167, pp. 809–814, 2011.

[59] A. Engel, A. Schilling, K. Ilin, and M. Siegel, "Dependence of count rate on magnetic field in superconducting thin-film TaN single-photon detectors," *Physical Review B*, vol. 86, Article ID 140506, 2012.

[60] A. J. Kerman, E. A. Dauler, W. E. Keicher et al., "Kinetic-inductance-limited reset time of superconducting nanowire photon counters," *Applied Physics Letters*, vol. 88, no. 11, Article ID 111116, 2006.

[61] G. Gol'Tsman, O. Okunev, G. Chulkova et al., "Fabrication and properties of an ultrafast NbN hot-electron single-photon detector," *IEEE Transactions on Applied Superconductivity*, vol. 11, no. 1, pp. 574–577, 2001.

[62] J. Zhang, W. Slysz, A. Verevkin et al., "Response time characterization of NbN superconducting single-photon detectors," *IEEE Transactions on Applied Superconductivity*, vol. 13, no. 2, pp. 180–183, 2003.

[63] C. M. Natarajan, M. G. Tanner, and R. H. Hadfields, "Superconducting nanowire single-photon detectors: physics and applications," *Superconductor Science and Technology*, vol. 25, no. 6, Article ID 063001, 2012.

[64] P. B. Miller, "Surface impedance of superconductors," *Physical Review*, vol. 118, no. 4, pp. 928–934, 1960.

[65] A. A. Abrikosov, L. P. Gorkov, and I. M. Khalatnikov, "A Superconductor in a high frequency field," *Soviet Physics: JETP*, vol. 8, no. 1, pp. 182–189, 1959.

[66] A. A. Abrikosov, L. P. Gorkov, and I. M. Khalatnikov, "Analysis of experimental data relating to the surface impedance of superconductors," *Soviet Physics: JETP*, vol. 10, no. 1, pp. 132–134, 1960.

[67] J.-J. Chang and D. J. Scalapino, "Gap enhancement in superconducting thin films due to microwave irradiation," *Journal of Low Temperature Physics*, vol. 29, no. 5-6, pp. 477–485, 1977.

[68] J.-J. Chang and D. J. Scalapino, "Kinetic-equation approach to nonequilibrium superconductivity," *Physical Review B*, vol. 15, no. 5, pp. 2651–2670, 1977.

[69] J.-J. Chang and D. J. Scalapino, "Nonequilibrium superconductivity," *Journal of Low Temperature Physics*, vol. 31, no. 1-2, pp. 1–32, 1978.

[70] D. N. Langenberg and A. L. Larkin, Eds., *Nonequilibrium Superconductivity*, North-Holland, Amserdam, The Netherlands, 1986.

[71] N. Kopnin, *Theory of Nonequilibrium Superconductivity*, Oxford University Press, Oxford, UK, 2009.

[72] U. S. Pracht, E. Heintze, C. Clauss et al., "Electrodynamics of the superconducting state in ultra-thin films at THz frequencies," *IEEE Transactions on Terahertz Science and Technology*, vol. 3, no. 3, pp. 269–280, 2013.

[73] L. Leplae, "Derivation of an expression for the conductivity of superconductors in terms of the normal-state conductivity," *Physical Review B*, vol. 27, no. 3, pp. 1911–1912, 1983.

[74] J.-J. Chang and D. J. Scalapino, "Electromagnetic response of layered superconductors," *Physical Review B*, vol. 40, no. 7, pp. 4299–4305, 1989.

[75] A. J. Berlinsky, C. Kallin, G. Rose, and A.-C. Shi, "Two-fluid interpretation of the conductivity of clean BCS superconductors," *Physical Review B*, vol. 48, no. 6, pp. 4074–4079, 1993.

[76] S. B. Nam, "Theory of electromagnetic properties of superconducting and normal systems. I," *Physical Review*, vol. 156, no. 2, pp. 470–486, 1967.

[77] S. B. Nam, "Theory of electromagnetic properties of strong-coupling and impure superconductors. II," *Physical Review*, vol. 156, no. 2, pp. 487–493, 1967.

[78] O. Klein, S. Donovan, M. Dressel, and G. Grüner, "Microwave cavity perturbation technique: part I: principles," *International Journal of Infrared and Millimeter Waves*, vol. 14, no. 12, pp. 2423–2457, 1993.

[79] S. Donovan, O. Klein, M. Dressel, K. Holczer, and G. Grüner, "Microwave cavity perturbation technique: part II: experimental scheme," *International Journal of Infrared and Millimeter Waves*, vol. 14, no. 12, pp. 2459–2487, 1993.

[80] M. Dressel, O. Klein, S. Donovan, and G. Grüner, "Microwave cavity perturbation technique: part III: applications," *International Journal of Infrared and Millimeter Waves*, vol. 14, no. 12, pp. 2489–2517, 1993.

[81] M. Scheffler and M. Dressel, "Broadband microwave spectroscopy in Corbino geometry for temperatures down to 1.7 K," *Review of Scientific Instruments*, vol. 76, no. 7, Article ID 074702, 2005.

[82] M. Scheffler, S. Kilic, and M. Dressel, "Strip-shaped samples in a microwave Corbino spectrometer," *Review of Scientific Instruments*, vol. 78, no. 8, Article ID 086106, 2007.

[83] K. Steinberg, M. Scheffler, and M. Dressel, "Broadband microwave spectroscopy in Corbino geometry at ^{3}He temperatures," *Review of Scientific Instruments*, vol. 83, no. 2, Article ID 024704, 2012.

[84] R. P. S. M. Lobo, J. D. LaVeigne, D. H. Reitze et al., "Photoinduced time-resolved electrodynamics of superconducting metals and alloys," *Physical Review B*, vol. 72, no. 2, Article ID 024510, 2005.

[85] K. E. Kornelsen, M. Dressel, J. E. Eldridge, M. J. Brett, and K. L. Westra, "Far-infrared optical absorption and reflectivity of a superconducting NbN film," *Physical Review B*, vol. 44, no. 21, pp. 11882–11887, 1991.

[86] D. Karecki, R. E. Peña, and S. Perkowitz, "Far-infrared transmission of superconducting homogeneous NbN films: scattering time effects," *Physical Review B*, vol. 25, no. 3, pp. 1565–1571, 1982.

[87] M. Šindler, R. Tesař, J. Koláček, L. Skrbek, and Z. ŠimŠa, "Far-infrared transmission of a superconducting NbN film," *Physical Review B*, vol. 81, no. 18, Article ID 184529, 2010.

[88] R. Tesař, M. Šindler, K. Ilin, J. Koláček, M. Siegel, and L. Skrbek, "Terahertz thermal spectroscopy of a NbN superconductor," *Physical Review B*, vol. 84, no. 13, Article ID 132506, 2011.

[89] M. W. Coffey and J. R. Clem, "Theory of high-frequency linear response of isotropic type-II superconductors in the mixed state," *Physical Review B*, vol. 46, no. 18, pp. 11757–11764, 1992.

[90] M. W. Coffey and J. R. Clem, "Theory of microwave transmission and reflection in type-II superconductors in the mixed state," *Physical Review B*, vol. 48, no. 1, pp. 342–350, 1993.

[91] B. P. Gorshunov, G. V. Kozlov, A. A. Volkov et al., "Measurement of electrodynamic parameters of superconducting films in the far-infrared and submillimeter frequency ranges," *International Journal of Infrared and Millimeter Waves*, vol. 14, no. 3, pp. 683–702, 1993.

[92] B. P. Gorshunov, I. V. Fedorov, G. V. Kozlov, A. A. Volkov, and A. D. Semenov, "Dynamic conductivity and the coherence peak in the submillimeter spectra of superconducting NbN films," *Solid State Communications*, vol. 87, no. 1, pp. 17–21, 1993.

[93] B. Gorshunov, A. Volkov, I. Spektor et al., "Terahertz BWO-spectrosopy," *International Journal of Infrared and Millimeter Waves*, vol. 26, no. 9, pp. 1217–1240, 2005.

[94] B. P. Gorshunov, A. A. Volkov, A. S. Prokhorov et al., "Terahetz BWO spectroscopy of conductors and superconductors," *Quantum Electronics*, vol. 37, no. 10, pp. 916–923, 2007.

[95] M. Dressel, N. Drichko, B. Gorshunov, and A. Pimenov, "THz spectroscopy of superconductors," *IEEE Journal on Selected Topics in Quantum Electronics*, vol. 14, no. 2, pp. 399–406, 2008.

[96] M. C. Nuss, K. W. Goossen, J. P. Gordon, P. M. Mankiewich, M. L. O'Malley, and M. Bhushan, "Terahertz time-domain measurement of the conductivity and superconducting band gap in niobium," *Journal of Applied Physics*, vol. 70, no. 4, pp. 2238–2241, 1991.

[97] A. V. Pronin, M. Dressel, A. Pimenov, A. Loidl, I. V. Roshchin, and L. H. Greene, "Direct observation of the superconducting energy gap developing in the conductivity spectra of niobium," *Physical Review B*, vol. 57, no. 22, pp. 14416–14421, 1998.

[98] U. Pracht, M. Scheffler, M. Dressel, K. S. Ilin, and M. Siegel,unpublished.

[99] A. Semenov, B. Günther, U. Böttger et al., "Optical and transport properties of ultrathin NbN films and nanostructures," *Physical Review B*, vol. 80, no. 5, Article ID 054510, 2009.

[100] E. Burstein, D. N. Langenberg, and B. N. Taylor, "Superconductors as quantum detectors for microwave and sub-millimeter-wave radiation," *Physical Review Letters*, vol. 6, no. 3, pp. 92–94, 1961.

[101] D. M. Ginsberg, "Upper limit for quasi-particle recombination time in a superconductor," *Physical Review Letters*, vol. 8, no. 5, pp. 204–207, 1962.

[102] J. R. Schrieffer and D. M. Ginsberg, "Calculation of the quasiparticle recombination time in a superconductor," *Physical Review Letters*, vol. 8, no. 5, pp. 207–208, 1962.

[103] A. Rothwarf and M. Cohen, "Rate of capture of electrons injected into superconducting lead," *Physical Review*, vol. 130, no. 4, pp. 1401–1405, 1963.

[104] A. Rothwarf and B. N. Taylor, "Measurement of recombination lifetimes in superconductors," *Physical Review Letters*, vol. 19, no. 1, pp. 27–30, 1967.

[105] L. R. Testardi, "Destruction of superconductivity by laser light," *Physical Review B*, vol. 4, no. 7, pp. 2189–2196, 1971.

[106] J. F. Federici, B. I. Greene, P. N. Saeta, D. R. Dykaar, F. Sharifi, and R. C. Dynes, "Direct picosecond measurement of photoinduced Cooper-pair breaking in lead," *Physical Review B*, vol. 46, no. 17, pp. 11153–11156, 1992.

[107] Experiments on NbN films by R. Kaindl, M. Carnahan, and D. Chemla at the Advanced Light Source of the Lawrance Berkeley National Laboratory. Figure reproduced from N. Gedik: THz spectroscopy of quasiparticle dynamics in complex materials, https://portal.slac.stanford.edu/sites/conf_public/THz_2012_09/presentations/gedik_Frontiers_of_THz_Science.pdf.

[108] M. Beck, M. Klammer, S. Lang et al., "Energy-gap dynamics of superconducting NbN thin films studied by time-resolved terahertz spectroscopy," *Physical Review Letters*, vol. 107, no. 17, Article ID 177007, 2011.

[109] R. Matsunaga and R. Shimano, "Nonequilibrium BCS state dynamics induced by intense terahertz pulses in a superconducting NbN film," *Physical Review Letters*, vol. 109, no. 18, Article ID 187002, 1 page, 2012.

[110] J.-J. Chang and D. J. Scalapino, "New instability in superconductors under external dynamic pair breaking," *Physical Review B*, vol. 10, no. 9, pp. 4047–4049, 1974.

[111] D. J. Scalapino and B. A. Huberman, "Onset of an inhomogeneous state in a nonequilibrium superconducting film," *Physical Review Letters*, vol. 39, no. 21, pp. 1365–1368, 1977.

[112] P. W. Anderson, "Theory of dirty superconductors," *Journal of Physics and Chemistry of Solids*, vol. 11, no. 1-2, pp. 26–30, 1959.

[113] M. Strongin, R. S. Thompson, O. F. Kammerer, and J. E. Crow, "Destruction of superconductivity in disordered near-monolayer films," *Physical Review B*, vol. 1, no. 3, pp. 1078–1091, 1970.

[114] R. C. Dynes, A. E. White, J. M. Graybeal, and J. P. Garno, "Breakdown of eliashberg theory for two-dimensional superconductivity in the presence of disorder," *Physical Review Letters*, vol. 57, no. 17, pp. 2195–2198, 1986.

[115] D. B. Haviland, Y. Liu, and A. M. Goldman, "Onset of superconductivity in the two-dimensional limit," *Physical Review Letters*, vol. 62, no. 18, pp. 2180–2183, 1989.

[116] J. M. Valles Jr., R. C. Dynes, and J. P. Garno, "Electron tunneling determination of the order-parameter amplitude at the superconductor-insulator transition in 2D," *Physical Review Letters*, vol. 69, no. 24, pp. 3567–3570, 1992.

[117] A. Yazdani and A. Kapitulnik, "Superconducting-insulating transition in two-dimensional a-MoGe thin films," *Physical Review Letters*, vol. 74, no. 15, pp. 3037–3040, 1995.

[118] A. M. Goldman and N. Marković, "Superconductor-insulator transitions in the two-dimensional limit," *Physics Today*, vol. 51, no. 11, pp. 39–44, 1998.

[119] M. A. Paalanen, A. F. Hebard, and R. R. Ruel, "Low-temperature insulating phases of uniformly disordered two-dimensional superconductors," *Physical Review Letters*, vol. 69, no. 10, pp. 1604–1607, 1992.

[120] V. F. Gantmakher, M. V. Golubkov, V. T. Dolgopolov, G. E. Tsydynzhapov, and A. A. Shashkin, "Destruction of localized electron pairs above the magnetic-field-driven superconductor-insulator transition in amorphous In-O films," *JETP Letters*, vol. 68, no. 4, pp. 363–369, 1998.

[121] V. Y. Butko and P. W. Adams, "Quantum metallicity in a two-dimensional insulator," *Nature*, vol. 409, no. 6817, pp. 161–164, 2001.

[122] V. F. Gantmakher, S. N. Ermolov, G. E. Tsydynzhapov, A. A. Zhukov, and T. I. Baturina, "Suppression of 2D superconductivity by the magnetic field: quantum corrections vs. the superconductor-insulator transition," *JETP Letters*, vol. 77, no. 8, pp. 424–428, 2003.

[123] N. Hadacek, M. Sanquer, and J.-C. Villégier, "Double reentrant superconductor-insulator transition in thin TiN films," *Physical Review B*, vol. 69, no. 2, Article ID 024505, 2004.

[124] G. Sambandamurthy, L. W. Engel, A. Johansson, and D. Shahar, "Superconductivity-Related Insulating Behavior," *Physical Review Letters*, vol. 92, no. 10, Article ID 107005, 2004.

[125] G. Sambandamurthy, L. W. Engel, A. Johansson, E. Peled, and D. Shahar, "Experimental evidence for a collective insulating state in two-dimensional superconductors," *Physical Review Letters*, vol. 94, no. 1, Article ID 017003, 2005.

[126] M. Steiner and A. Kapitulnik, "Superconductivity in the insulating phase above the field-tuned superconductor-insulator transition in disordered indium oxide films," *Physica C*, vol. 422, no. 1-2, pp. 16–26, 2005.

[127] T. I. Baturina, J. Bentner, C. Strunk, M. R. Baklanov, and A. Satta, "From quantum corrections to magnetic-field-tuned superconductor-insulator quantum phase transition in TiN films," *Physica B*, vol. 359-361, pp. 500–502, 2005.

[128] T. I. Baturina, C. Strunk, M. R. Baklanov, and A. Satta, "Quantum metallicity on the high-field side of the superconductor-insulator transition," *Physical Review Letters*, vol. 98, no. 12, Article ID 127003, 2007.

[129] B. Sacépé, C. Chapelier, T. I. Baturina, V. M. Vinokur, M. R. Baklanov, and M. Sanquer, "Disorder-induced inhomogeneities of the superconducting state close to the superconductor-insulator transition," *Physical Review Letters*, vol. 101, no. 15, Article ID 157006, 2008.

[130] B. Sacépé, T. Dubouchet, C. Chapelier et al., "Localization of preformed Cooper pairs in disordered superconductors," *Nature Physics*, vol. 7, no. 3, pp. 239–244, 2011.

[131] S. M. Hollen, H. Q. Nguyen, E. Rudisaile et al., "Cooper-pair insulator phase in superconducting amorphous Bi films induced by nanometer-scale thickness variations," *Physical Review B*, vol. 84, no. 6, Article ID 064528, 2011.

[132] V. M. Vinokur, T. I. Baturina, M. V. Fistul, A. Y. Mironov, M. R. Baklanov, and C. Strunk, "Superinsulator and quantum synchronization," *Nature*, vol. 452, no. 7187, pp. 613–615, 2008.

[133] S. Poran, E. Shimshoni, and A. Frydman, "Disorder-induced superconducting ratchet effect in nanowires," *Physical Review B*, vol. 84, no. 1, Article ID 014529, 2011.

[134] Y. Dubi, Y. Meir, and Y. Avishai, "Theory of the magnetoresistance of disordered superconducting films," *Physical Review B*, vol. 73, no. 5, Article ID 054509, 2006.

[135] Y. Dubi, Y. Meir, and Y. Avishai, "Nature of the superconductor-insulator transition in disordered superconductors," *Nature*, vol. 449, no. 7164, pp. 876–880, 2007.

[136] D. Kowal and Z. Ovadyahu, "Disorder induced granularity in an amorphous superconductor," *Solid State Communications*, vol. 90, no. 12, pp. 783–786, 1994.

[137] D. Kowal and Z. Ovadyahu, "Scale dependent superconductor-insulator transition," *Physica C*, vol. 468, no. 4, pp. 322–325, 2008.

[138] N. Trivedi, R. T. Scalettar, and M. Randeria, "Superconductor-insulator transition in a disordered electronic system," *Physical Review B*, vol. 54, no. 6, pp. R3756–R3759, 1996.

[139] Y. Imry, M. Strongin, and C. C. Homes, "An inhomogeneous Josephson phase in thin-film and high-T_c superconductors," *Physica C*, vol. 468, no. 4, pp. 288–293, 2008.

[140] M. V. Feigei'man, L. B. Ioffe, V. E. Kravtsov, and E. A. Yuzbashyan, "Eigenfunction fractality and pseudogap state near the superconductor-insulator transition," *Physical Review Letters*, vol. 98, no. 2, Article ID 027001, 2007.

[141] M. V. Feigel'man, L. B. Ioffe, V. E. Kravtsov, and E. Cuevas, "Fractal superconductivity near localization threshold," *Annals of Physics*, vol. 325, no. 7, pp. 1390–1478, 2010.

[142] K. Bouadim, Y. L. Loh, M. Randeria, and N. Trivedi, "Single- and two-particle energy gaps across the disorder-driven superconductor-insulator transition," *Nature Physics*, vol. 7, no. 11, pp. 884–889, 2011.